Computers in Biology and Medicine 111 (2019) 103340

Contents lists available at ScienceDirect

Computers in Biology and Medicine

journal homepage: www.elsevier.com/locate/compbiomed

NGRID: A novel platform for detection and progress assessment of visual distortion caused by macular disorders

Navid Mohaghegh[a,b], Ebrahim Ghafar-Zadeh[a,b,*], Sebastian Magierowski[b]

[a] Biologically Inspired Sensors and Actuators (BioSA) Laboratory, Canada
[b] Department of Electrical Engineering and Computer Science, Lassonde School of Engineering, York University, Toronto, Canada

ARTICLE INFO

Keywords:
Macular disorders
Scalable vector graphics (SVG)
Central serous retinopathy (CSR)
Graphical macular interface system (GMIS)
Age-related macular degeneration (AMD)

ABSTRACT

This paper presents a new graphical macular interface system (GMIS) for accurate, rapid, and quantitative measurement of visual distortion (VD) in the central vision of patients suffering from macular disorders. In this system, a series of predefined graphical patterns or multiple grids (NGRID) are randomly selected from a library of patterns and visualized on the screen, then the VDs identified by the patient are recorded as binary codes using various control methods including speech recognition. Scalable Vector Graphics (SVG) is used to generate the patterns and save them into a central library. Based on the projected patterns and the patients' responses, a VD graph or so-called heatmap is generated for eye-care purposes. We demonstrate and discuss the functionality of the proposed system for the detection and progress assessment of a macular condition in patients suffering from Central Serous Chorioretinopathy (CSR). Also, we characterize the proposed technique to evaluate the systematic error and response time on healthy human subjects with normal vision. Based on these results, the voice recognition input method exhibits a lower error but a higher response time compared to other input devices. We run the proposed NGRID VD technique to evaluate the effect of CSR on the visual field of a CSR patient. The generated heatmaps are in agreement with standard Optical Coherence Tomography (OCT) images obtained at different times from both the left and right eyes. These results reveal the applicability of the proposed technique for the detection and assessment of macular disorders. Based on these results, the proposed NGRID platform shows great promise for use as an alternative solution for in-home monitoring of various macular disorders and as a means of forwarding responses to secured cloud facilities for future data analysis.

1. Introduction

Macular disorders such as Myopic Maculopathy, Macular Holes, Diabetic Macular Edema, Age-Related Macular Degeneration (AMD), and Central Serous Chorioretinopathy (CSR) affect central vision [1–3]. In their early stages, they cause Visual Distortion (VD) including metamorphopsia [4]. In their advanced phases, they cause severe VD, including central vision loss and scotoma. Among these retinal disorders, AMD is the leading cause of blindness, and it has been projected to affect 196 million people over the age of 65 worldwide by 2020, and up to 288 million by 2050 [5]. Early detection of macular disorders is crucial as close monitoring allows for intervention before irreversible damage occurs [6,7]. As seen in Fig. 1, at their early stage, these conditions mainly inflict retinal deformation, subsequently causing mild to severe VDs.

The Amsler chart, a printed paper grid with a central fixation mark, is widely used to test visual abnormalities [8]. Current best practice for patients relies on measuring their responses to an Amsler chart test followed by an immediate assessment of their performance to perceive any new developed VDs, as seen in Fig. 2a. However, the sensitivity of the Amsler chart in detecting small VDs is low (50% failure on VDs smaller than 6° [9]). Also, the detected VD results are not numerical and fall to the interpretation of the test administrator. Therefore, it is not possible to quantify the progress of the macular disorder.

Many papers have recently reported the advantages of computerized methods to overcome the problems mentioned above [2,10–13]. Among these, graphical techniques and tests such as Preferential Hyperacuity Perimeter (PHP) and Macular Computerized Psychophysical Test (MCPT) have recently received interest from eye care professionals [11,14–16]. In MCPT, the patient is asked to direct a cursor to a point in the center of the screen using a mouse prompting the system to generate a virtual line [11,14]. Assuming the virtual line is projected in the retina lesion, subsequent a rapid fixation, the patient should be able to detect the VD. The PHP technique similarly generates stimuli consisting

* Corresponding author. Biologically Inspired Sensors and Actuators (BioSA) Laboratory, Canada.
E-mail address: egz@yorku.ca (E. Ghafar-Zadeh).

https://doi.org/10.1016/j.compbiomed.2019.103340
Received 8 October 2018; Received in revised form 20 June 2019; Accepted 20 June 2019
0010-4825/

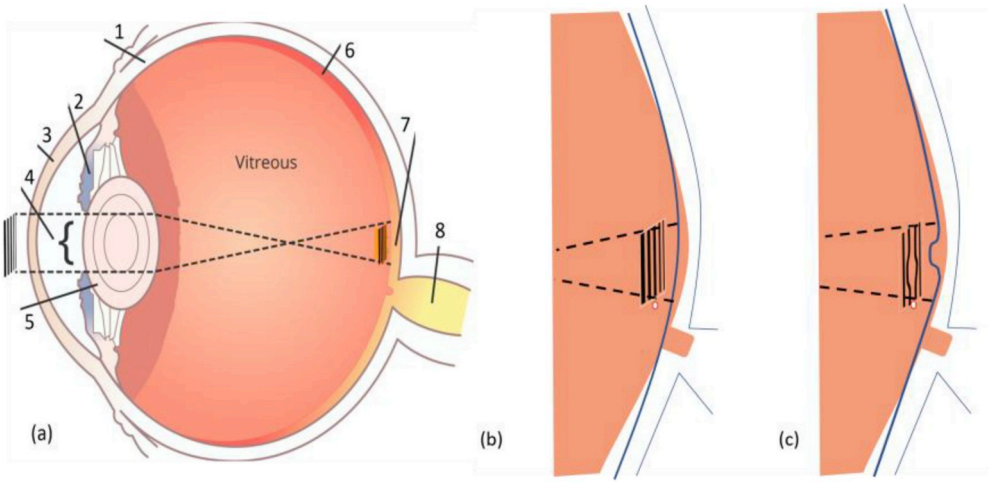

Fig. 1. Schematics of (a) a retina with (b) healthy macula versus (c) unhealthy macula (the deformed retinal basement due to macular disorder). Various parts of the eye including (1) sclera, (2) iris, (3) cornea, (4) pupil, (5) lens, (6) entire retina, (7) macula, (8) optic nerve and vitreous are shown in this figure.

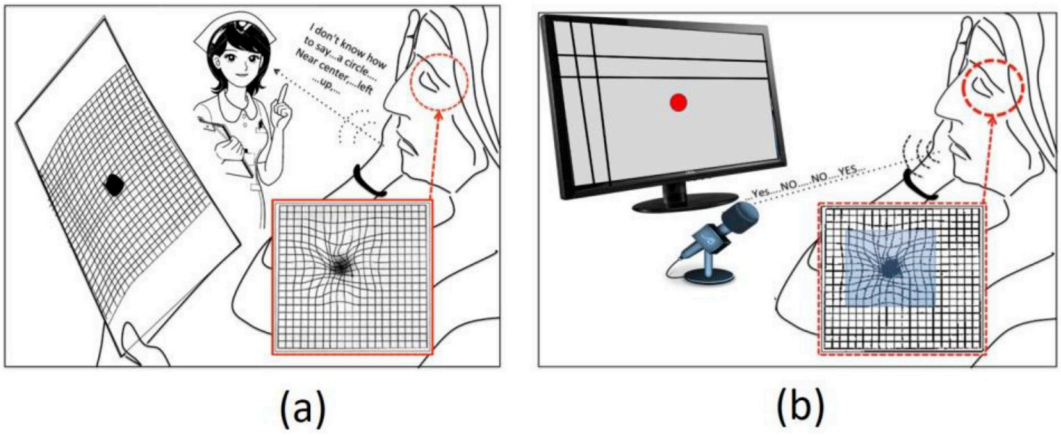

Fig. 2. Schematics of (a) legacy paper-based Amsler grid VD detection, versus (b) quantitative computerized VD detection.

of a straight line of dots with one or two dots out of alignment. These misalignments should be subsequently identified by touching the screen using a stylus pen [17,18].

The aforementioned techniques offer several advantages including low complexity, non-invasiveness, and home diagnostic capabilities. However, they still suffer from some limitations. For instance, the accuracy of the above techniques to identify the position of retinal lesions depends on the proper visual fixation at the center of the screen. In these techniques, the patients' focus moves from the center of the screen to find the position of the mouse cursor (MCPT method) or the stylus pen (PHP method) to touch the screen. This results in rapidly changing fixation between the center of the screen and input device. This repetitive change of fixation reduces the concentration of the patient and diminishes the accuracy of VD detection. This also increases the required time of examination as the patient becomes involved in the pointing task itself while executing the test. This issue can be studied through the Index of Difficulty via Fitts' Law [19]. Any pointing tasks, such as clicking between two points on the screen, possess a systematic inherent difficulty. Fitts' Law states that the pointing task becomes more difficult if smaller targets with more distance between them need to be targeted. Of course, not having any pointing task involved in the test would eliminate this inherent difficulty.

It is noteworthy that the examination time is an important factor that should be concise to avoid eye fatigue. In this paper, we propose a new graphical macular interface system (GMIS) for highly accurate detection of VDs caused by macular conditions. Fig. 2b illustrates the proposed technique which involves screening an array of patterns. A series of responses associated with the patterns are recorded in the form of binary data. Indeed, a series of positive (e.g. 'yes', 'good') or negative (e.g. 'no', 'bad') responses are collected and converted to a series of '0's and '1's respectively. In this process, binary data – '0', '1' – represents the absence ('good') or presence ('bad') of distortion in each projected pattern in the retina.

The main objective of this work is to develop a low cost, low complexity, easy to use, home monitoring device that can help patients to monitor the progress of their macular disorders and to have better measures by which to be alerted to visit the doctor's office. Such a unified hardware-software system needs to accurately and quickly perform the VD tests via GMIS to detect and monitor the progress of VDs, and consequently automatically alert the patient about the urgency to visit the doctor's office or the hospital, should Anti-VEGF injections or other procedures be needed [20]. The long-term objective of this work is the development of a data center that can collect the AMD assessment results and securely store the data in cloud servers. In this direction, we develop the required hardware as well as software to allow patients around the world to use the proposed platform to assess the progress of their macular disorder individually and to provide the opportunity for them to make their information available in support of data analysis efforts aimed at treating macular disorders for all. To date, a few papers reported the development of medical data [21,22] for

various biomedical applications but the development of a central data repository for macular disorders or retinal diseases have not been met yet. The focus of this paper is placed on developing a new method of detecting macular disorders using a unified software-hardware system. This custom-made platform will be employed for running the tests on a large number of patients suffering from various macular disorders, including CSR and AMD. This paper also paves the way for the development of such a central data resource after running the required clinical trials involving patients suffering from different macular disorders and also after receiving the standard health approvals. Macular related data collections derived from this research in the future might be suitable for ophthalmology research and pharmaceutical studies.

In the remainder of this paper, we put forward the proposed system in section II. In sections III and IV, we discuss the proposed hardware and software, respectively. In section V, we demonstrate and discuss the measurement results, followed by a conclusion in section VI.

2. Proposed interface system

The proposed GMIS relies on displaying predefined patterns and collecting patient responses using control devices. Based on the patterns and patient responses, a heatmap is generated for the detection and progress assessment of a macular condition. Below we discuss the details for each component comprising our proposed system including an overview of the patterns, use of control input devices to provide ways to answer the test, as well as different techniques to create the heatmap of visual distortions for visual and quantitative assessment of macular disorders.

2.1. Patterns

A GMIS includes a series of patterns that are used as stimuli projected onto the retina. The patient's response is recorded while the patient has concentrated their gaze onto the center of the screen. In order to avoid the problem of changing the fixation during the examination, in this work, a series of patterns are shown, and the patient is asked to react only if the predefined pattern is observed as being distorted. In other words, the proposed method does not require capturing the position of each distorted pattern via mouse or stylus. Let us assume a VD test is composed of a series of N frames that are visualized, and the patients' responses are recorded correspondingly. In each frame displayed to the patient, a pattern is displayed. This pattern can be a single or a group of straight-lines with predefined Cartesian coordinates, as seen in Fig. 3.

There are several parameters that can be selected to generate various patterns using straight lines, as seen in Fig. 3a–f. These parameters include width (W), length (L), grayscale (G) or colour (C), angle (α) and style (S) form of lines (e.g., solid, dash, dash-dot, etc.). A number (n) of parallel lines can form a pattern (Fig. 3e) or a network of patterns (Fig. 3f). The number of frames (N) and the time of projection (t_p) can be controlled by knowing the permitted time of examination. The optimum values of parameters are obtained for a high accuracy assessment of VDs. For instance, as the default, black lines on a white canvas are chosen to achieve the highest contrast. However, for patients who have difficulty recognizing such patterns, the system can further adjust colours, thickness, contrast, and brightness appropriately for each patient.

Additionally, the length and number of parallel lines, are two other parameters that can be modified to ease VD detection. Detecting misalignments in longer dashed lines are easier due to Vernier acuity in humans. Fig. 3g-l illustrate simplified models of distorted patterns, namely ξ_1, ξ_2, ξ_3, ξ_4, ξ_5 and ξ_6, respectively. One may argue that ξ_2 can be identified more easily than ξ_3 and ξ_1 (increasing contrast and presence of thicker multi patterns). Also, ξ_5 can be more easily detected than ξ_4 and ξ_6 with a healthy eye. Fig. 3c and 3i show patterns that can be repeated with different angles (α) in different positions. A series of such patterns are shown to the patient (see Fig. 3m). The combination of patterns shown in Fig. 3a-l can be used to form a VD test frame (one or more patterns can be used). The selected patterns from any one of the patterns in Fig. 3a–f should allow the accurate detection of visual distortion. For instance, a dotted line can be better detected than a solid line due to Vernier acuity (as utilized in PHP and MCPT methods). It is noteworthy that the parameters shown in Fig. 3 are changed per frame and VD test. These parameters show the flexibility of a graphical platform to develop multi-parameter patterns.

As noted above, a VD test includes a group of frames with straight lines; however, we have also used distorted lines to run a VD test on healthy participants to evaluate systematic errors and response times using various control devices. It is noteworthy that in each frame with a positive response, all Cartesian Coordinates points of a pattern are recorded. In this work, we take advantage of SVG for the generation of patterns, frames, and the collection of responses [23,24].

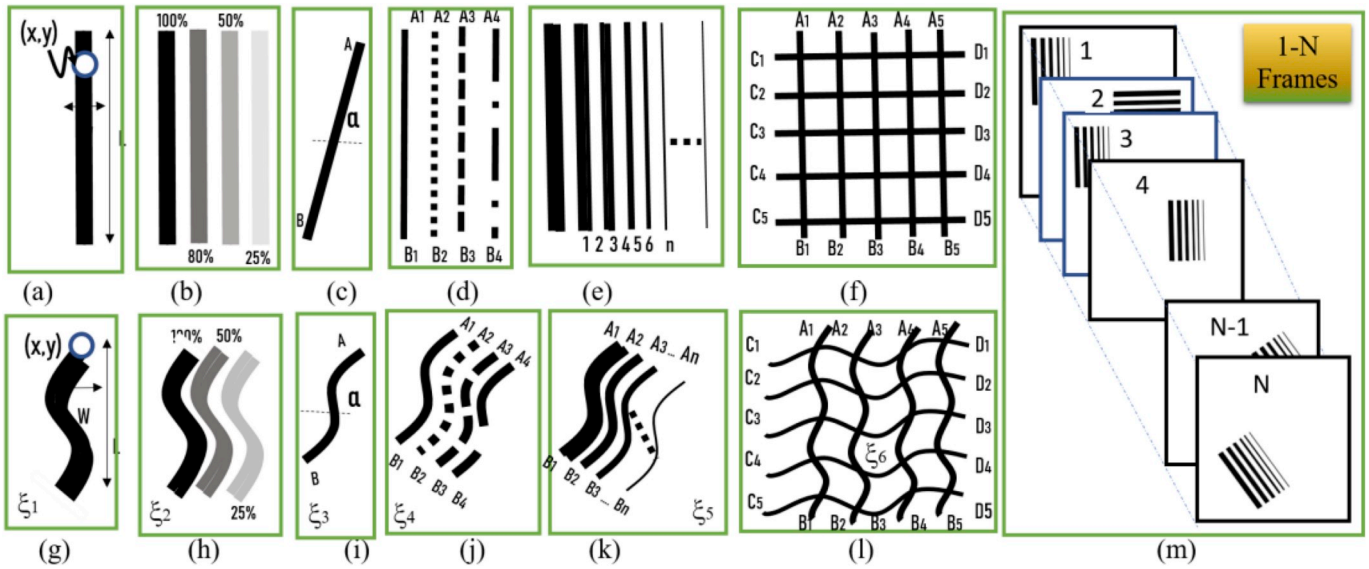

Fig. 3. Illustration of various patterns created with (a)–(f) straight lines and (g)–(l) distorted lines along with (m) a series of frames. The graphical pattern in each figure (g–l) are called ξ_1 –ξ_6 respectively.

2.2. Control

As mentioned, the response of a patient is recorded using a control input device, including keyboard, joystick, and speech recognition. The response of a patient for each one of the N frames can be '0' or '1'. At the end of an examination, N bits should be collected if a response is registered for all frames. All patterns associated with '1' bits will be used to create the heatmap. For the selection of an appropriate control device for a patient, the response time and error are two metrics that should be minimized. A characterization study has been made in the last section of this paper for the comparison of response times and errors in healthy participants. Among the control devices, speech recognition has the advantage of collecting the responses of patients for various patterns. For example, it can be used to identify the letters from the vocal responses of patients when the letters are used instead of patterns in a frame of the test.

2.3. Heatmap

As already mentioned, the recorded responses include a series of 0's and 1's that are used for VD assessment. This assessment can be performed using different methods to approximately calculate the boundary of metamorphopsia or scotoma. This boundary can be estimated using various methods including threshold, interpolation, or the proposed heatmap methods as seen in Fig. 4a–c. In this work, we will only use the heatmap method shown in Fig. 4c.

Threshold method: In this method, the number of 0's, regardless of the positions of associated patterns projected in the retina, can be counted and compared with a threshold number (Fig. 4a). This number should be higher than the systematic error. It is noteworthy that the systematic error is defined as the average number of errors made by participants with healthy eyes. This method can be used to detect the onset or to measure the progress, of macular conditions. However, it does not give any information about the location of lesion regions in the eye.

Interpolation method: In each VD test, the set of a patient's responses is used to create a boundary function. The boundary can be created by connecting the centers of all 'bad'-response patterns (Fig. 4b), which gives an estimate of the affected retinal lesions by calculating the surface of the boundary. However, this method suffers from a lack of accuracy since the center of each pattern is not necessarily placed in the VD affected lesion.

Heatmap method: In this method, all patterns that are related to the 'bad' responses are collapsed in a single frame. All pixels associated with the distorted patterns are used in the generation of a heatmap. Each pixel may belong to γ distorted patterns where $0 \leq \gamma$. The heatmap is generated by drawing a circle on each pixel so that each circle has an opacity and a radius proportional to γ (Fig. 4c). Therefore, the higher the γ, the higher the probability of identifying the damaged area in the retina. When a pattern is seen distorted, all pixels in the pattern are considered part of the damaged area even if only a single line or a pattern with multiple straight-lines is seen distorted. In this work, we use this method and a program, namely the NGRID Heatmap Generator. This method is discussed in section IV-F.

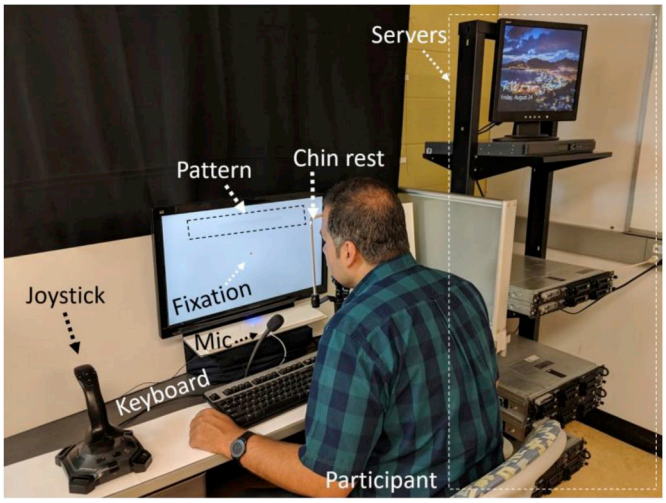

Fig. 5. A photograph of the NGRID platform including servers, control input devices (joystick, keyboard, microphone for speech recognition), monitor and a human participant who has fixated at the center of the screen (fixed his head in front of the screen using a chinrest

3. Implementation of NGRID hardware platform

In this section, we discuss the essential elements needed to create a hardware platform to facilitate NGRID tests and also securely store the data potentially collected from a broad population of patients using the system outside the clinic. Our main goal is to offer a low cost, easy-to-use home-based VD assessment method for patients suffering from macular conditions. Therefore, we developed a hardware platform to allow patients with an internet connection to perform their VD test daily or even several times per day. This platform includes a so-called NGRID Data Center that can also be used as a data processing facility for many applications, including the discovery of the effectiveness of various drugs and supplements.

3.1. NGRID servers

The NGRID Data Center is composed of a set of physical servers to create the cloud infrastructure that allows for linear scaling of NGRID when the anticipated scaling is needed for serving a large number of patients across the globe. As seen in Fig. 5, in this work, seven servers are utilized. This figure also conveys the test setup that is used to

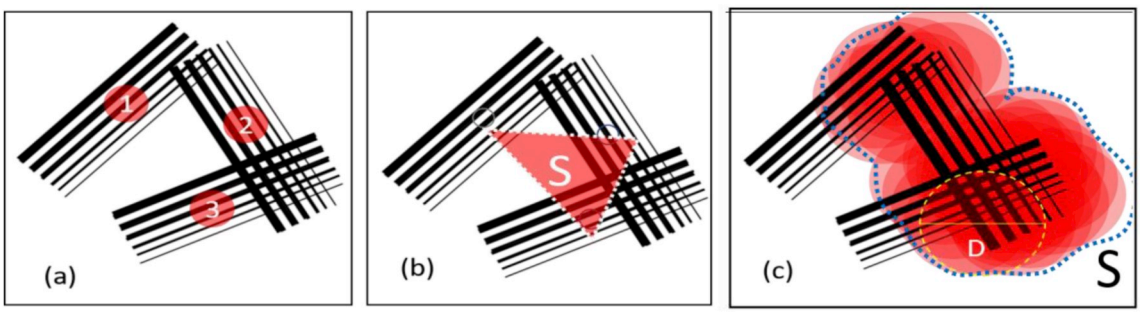

Fig. 4. Data Analysis strategies for creating the heatmap of the affected visual field; (a) threshold method, (b) interpolating method and (c) heatmap method. For simplicity, only the transparent circles associated with pixels possessing two crossing patterns.

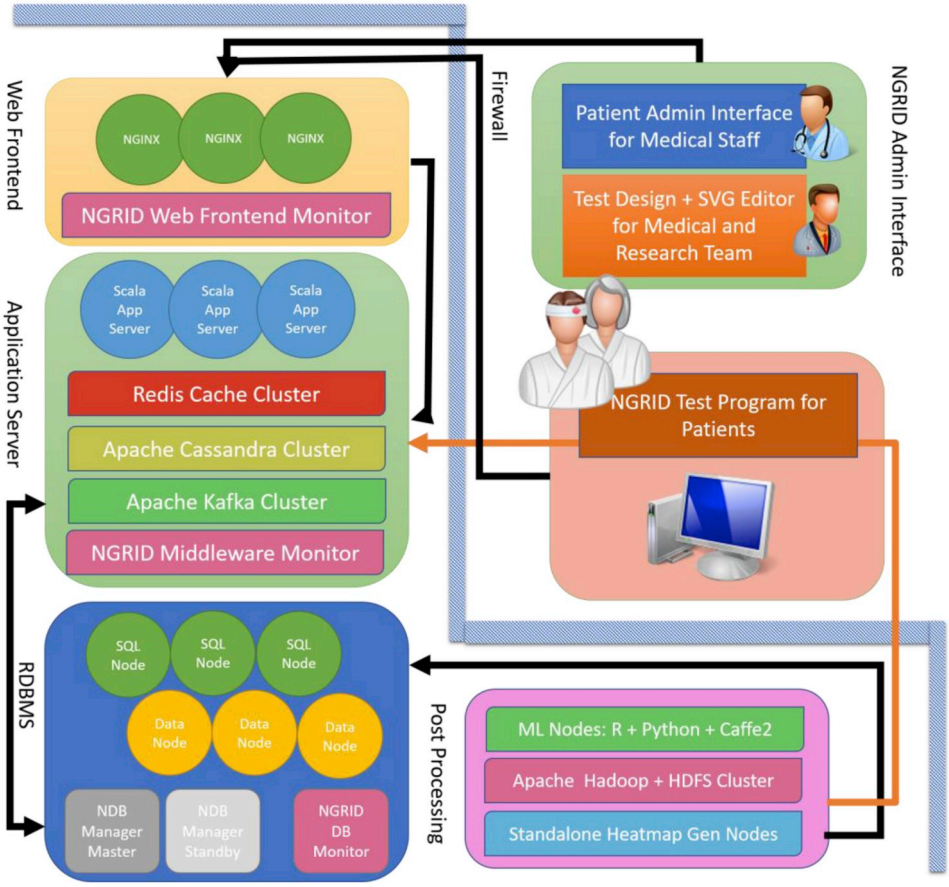

Fig. 6. Illustration of proposed software architecture.

perform all experiments described in section V. The actual home monitoring tests are performed in a slightly different environment and consequently the estimated accuracy and response time of the proposed method might be different. Each server has 64 GB of RAM and two physical Intel Xeon 5460 CPUs. The servers are also equipped with a 4 Gbps Host Bus Adapter (HBA) card to access the NGRID Storage Area Network (SAN). Each server runs on Linux Kernel 4.8 with the support of Linux Containers (LXC) for OS-Level Virtualization and also allows for Linux Virtual Server (LVS) to perform load detecting, fault tolerance and load balancing of services. Each server is equipped with TCP off-load and a Crypto Accelerator card (Cavium Nitrox) to accelerate the SSL/TLS process for secure communication. Servers are also connected through a backplane of a Host Channel Adapter (HCA) using Mellanox InfiniBand (IB) with Remote Direct Memory Access (RDMA) for in-cluster storage access and IP over IB (IPoIB) for fast 20 Gbps IP communication within the cluster.

In this work, we run multiple services using LXC to fully utilize each server. The services are composed of an SQL Database, Data Nodes along with SQL workers and DB cluster managers, NGINX Web Server acting as a static server while performing reverse proxy on the dynamic web requests to the NGRID Application Server written in Scala. We also use LXC to host Apache Cassandra and Spark nodes/workers for data crawling across the cluster to run our various analytics in the future. Our LXC also hosts the Apache Shiro security platform, which provides full SSL/TLS hardening and Single-Sign-On (SSO). Redis is utilized as an in-memory distributed cache for any small to medium size IO intensive scripts, using NoSQL. With the help of LVS (through persistent hashing, port health check, and monitoring the least established connections), we perform load-balancing and provide high availability. Through Apache Spark and LVS/LXC containers, the cluster can support a nearly linear growth in servers to handle the more NGRID traffic load.

3.2. Data storage

In our current prototype, to provide highly available storage for our micro-scaled NGRID data center cluster, we are connecting 20 × 300 GB SAS 6.0 Gbps 15 k RPM hard disk drives (with 4 × 128 GB solid state drives acting as a dedicated cache) to a cluster of active/passive OpenZFS links (via HBA 4 Gbps). To expose the LUNs to the NGRID cluster (hosted on OpenZFS), we use a 24 port SAN Surfer switch (connected to each server in the cluster via a 4 Gbps fibre channel link). Each OpenZFS pool has a dedicated SSD cache along with ZFS Intent Log (ZIL) to accelerate synchronous write transactions. LZ4 compression and deduplication are enabled.

In the NGRID platform, as mentioned in the next section, each test can produce as much as 10 MB of very detailed log files and around 8 MB of raw voice recording for each test that a patient undergoes. For 350 patients who simply perform the test 3 times per day around 7 TB of raw storage is needed to retain yearly data, which is lower than the capacity of dedicated hard drives in this platform. However, by increasing the number of patients, larger data storage is required. For this reason, in order to avoid dealing with large and costly storage needs, we enabled GZIP compression on our collected data (since the patient is not speaking constantly we achieved around 400–500% reduction in file sizes for our recordings). Also, the same was done for the stream of events and SQLite logs (since only raw ASCII logs with fairly repetitive keywords are used, a compression ratio of 700–800% is possible). This means our storage size can be reduced by a factor 5.5, thus needing in the range of 6 TB for five years' usage. Therefore, the dedicated hard drives (which use compression and deduplication at cluster level) are sufficient for this purpose. It is noteworthy that the real-time voice recognition is performed on a stream of PCM u8 mono channel at 11,025 samples per second with 8 bits per sample. Therefore, the audio

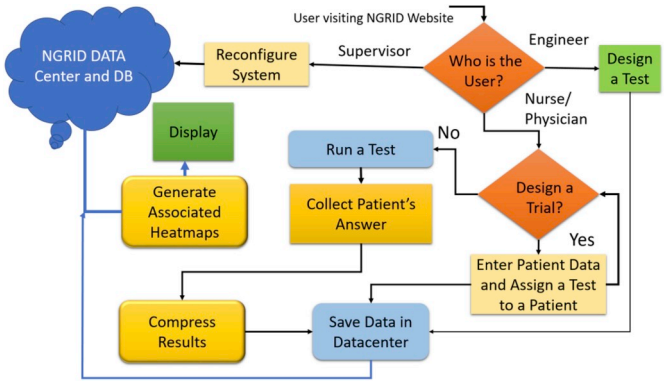

Fig. 7. The flowchart diagram of the proposed NGRID software platform.

file size for a 12-min recording with 11,025 samples per second and eight-bit resolution requires about 7.57 MB of storage space.

3.3. Other considerations related to display monitors

There are several parameters, such as luminance, contrast ratio, reflection, and viewing angle, that should be taken into account in the selection of medical displays [25]. In the proposed NGRID test, medical grade monitors with the capability of HFFS (High-Transmittance Fringe Field Switching) or AFFS+ (Advanced Fringe Field Switching) [26], for enhanced colour calibration, near optimal colour and luminosity reproduction and minimum colour distortion can significantly increase the accuracy of clinical trial tests. However, in the first stage of this work due to budgetary constraints, we used a regular monitor.

4. Implementation of NGRID software platform

In this section, we discuss the details of NGRID software for generating the patterns, projecting the patterns in the form of VD tests before healthy and unhealthy participants, collecting responses, design of user interfaces for entering participants' information and modifying the specification of NGRID programs and generating heatmaps for the attention of medical practitioners and ophthalmologists.

4.1. Software components

A simplified diagram of the proposed software architecture can be seen in Fig. 6. As shown, an administrative interface was developed to allow the research team along with medical staff, to easily create VD tests. Another administrative interface was developed to enable medical practitioners to add patients into the system and assign them different VD tests. Another program was developed for patients to perform VD tests. This program can also administer the VD test and collect the patient's answers for generating the heatmap. All aforementioned interfaces should be run securely in a highly distributed fashion in order to enable access to different hospitals in different geographic locations. To address this, as we discussed in section III, we created NGRID cloud servers to host and enable the above-developed interfaces. NGRID cloud servers are shielded through firewall, authentication, and authorization layers to safeguard access.

The web requests are reverse proxied through a cluster of highly available NGINX web servers that act as our Web Fronted layer. This layer is composed of various web server modules to validate and proxy communications to the backend Application Servers. The Application Servers provide the logic and all the interfaces that are used by NGRID VD Tests, NGRID SVG Editor, and NGRID Admin Interface. This layer is composed of a dynamically scalable sub-cluster of NGRID Scala Application Servers. In this platform, we are required to cache the most frequently used data and thus decided to use an in-memory Redis cluster to achieve this goal.

Further, this software system needs to store raw test events and data, and we thus decided to use an Apache Cassandra cluster to achieve this goal along with Apache Kafka streams to communicate all the test events to the underlying Post Processing layer. To store the tests' graphical data and settings, we should develop a Relational Database Management System (RDBMS) and create a highly available Network Database layer (NDB). A MySQL cluster is used as our RDBMS backend which is composed of a series of scalable nodes to store the data (data nodes), to provide means to process SQL queries (SQL nodes), and provide a management system to scale-up and monitor the NDBs (NDB manager nodes). Once patients do a VD test and all test answers and events are collected, we need to process the patients' answers and find the areas wherein they experience visual distortion. We do this at the Post Processing layer, which goes through all the stored answers and generates a heatmap to visualize the severity of VD areas experienced by each patient. Furthermore, within the post-processing layer, we created a highly available and scalable Apache Hadoop and Spark cluster to allow deep learning for our future needs (e.g., provide means to analyze the collected data across hospitals to determine the effectiveness of various treatments).

4.2. NGRID flow chart

As seen in Fig. 7, this platform allows users, including patients or ophthalmology assistants or supervisors, access to the platform. At the first step, the users are identified as (a) supervisor, (b) patient/assistant or physician or (c) software designer. A designer can develop new patterns and generate new VD tests using the proposed web-based tool introduced in sub-section IV-C. The generated data is saved in the Data Center and collected in the Database (DB). The NGRID data center has many other components which are responsible for processing the results and generating heatmaps as well as a secure, load-balanced, web portal to access NGRID admin and patient components. A summary of NGRID Data Center programs is mentioned in Table 1.

As shown in Fig. 7, the supervisor can reconfigure the system parameters including retention of the stored log files as well as adding new designers and physician login credentials to the system as briefly mentioned in subsection IV-A.

An important part of the system is the means of offering access to

Table 1
A summary of programs developed in the Software platform.

Name of Program	Language	Input/Process/Output
NGRID Test App	C++ and C#	Consumes stored tests patterns and produces raw test results in NGRID datacenter.
NGRID Database	SQL and NoSQL	A highly available database within NGRID datacenter that keeps all test data, credentials, and test results.
NGRID SVG Editor	HTML5, CSS3 and JavaScript	Facilitates creating various SVGs that compose patterns used in NGRID Tests. The outputs are store in NGRID database
NGRID Admin	Scala, Java, HTML5/CSS3 and JavaScript	This website allows for physicians and admins to login and produces and control various NGRID Tests.
NGRID Heatmap Generator	R, C#, C++, OpenCV, HTML5, CSS3 and JavaScript	Consumes raw test results and after various rasterization and image processing, produces heatmap results for a test that a patient has completed.

patients or eye-care professionals by which to design a trial or to run a test. A trial is designed by entering the patient's information and setting a specific VD test. A patient can be allocated to different trials with different ID numbers. The trials are saved in the database of the NGRID data center. Once the trial is designed and the test is set to a particular patient, the patient can '*run the test*'. In this test, a series of frames are displayed, and the patient's responses are collected, compressed, and saved in the data center. The VD test result can be displayed in the form of a heatmap using the data saved in the data center. In this platform, several programs were developed using different programming techniques. A summary of these programs is shown in Table 1, and details are discussed in following subsections IV-D, IV-E, and IV-F.

4.3. VD test editor design and integration with data center

Scalable Vector Graphics (SVG) [23] is used to create complex graphical patterns. SVG is a royalty-free and widely used standard that is supported by many web browsers, including those used in mobile phones and tablets. This allows the custom made NGRID SVG patterns to be displayable in commodity hardware without the need to pay royalty fees. This is an important factor in developing low-cost software for home diagnostics purposes. Furthermore, SVG is completely independent of the resolution of the underlying rendering device which allows for VD tests to be easily scaled for any screen sizes, pixel densities or different Head Mounted Displays (HMD) that can be afforded by hospitals and doctors' offices. As an example, a simple SVG program (see SVG Program 1) is shown below for drawing a dashed line or so-called line001 from Cartesian coordinates ($x_1 = 100$, $y_1 = 100$) to ($x_2 = 400$, $y_2 = 200$) in canvas with width and height of 500 pixels at a scale of 1.0 without any magnification.

SVG Program 1: Drawing simple patterns

```
<svg width="500" height="500" xmlns="http://www.w3.org/2000/svg">
    <line id="line001" x1="100" y1="100"
                       x2="400" y2="200"
                       stroke-dasharray="2,2" stroke-width="1.0"
                       stroke="#000000" />
</svg>
```

Since SVGs are based on the Extensible Markup Language (XML), the arrangements of each pattern can be programmatically scripted and changed via the manipulation of the SVG Document Object Model (DOM) [24]. DOM manipulation provides a very powerful feature to NGRID that allows sophisticated graphical shapes to be designed, animated and scripted mathematically. NGRID creates extended APIs that allow easy manipulation of SVG DOM. This allows NGRID to create shapes that are purely stated in terms of mathematical expressions. NGRID DOM manipulation also allows for the creation of sophisticated VD graphic tests via a program that generates and controls various SVG shapes and their attributes (e.g., location, scale and various style actors such as colour, thickness, and transparency). This means that mathematical expressions and the shapes of the patterns they described can be further modified through the NGRID API. A sample NGRID custom API for DOM manipulation is shown below (see SVG Program 2) to change line001 coordinates from ($x_1 = 0$, $y_1 = 0$) to new ($x_1 = 50$, $y_1 = 50$) as well as the colour of the line from black to red. As seen in the above program, once the first part of the code is executed, it results in the transformation of the original SVG. Indeed, SVGs can be created simply by writing text files that conform to the SVG standard. Since SVG creation can be time-consuming and prone to human coding errors, NGRID has addressed this issue by providing an enhanced customized online SVG Editor that allows ways to create and modify the pattern of each frame in a fully graphical way without the need to write SVG code as seen in Fig. 8. This will ease the process of pattern generation for NGRID VD tests. The NGRID SVG Editor is a web-based system that allows for easy and rapid creation as well as a means for saving the tests online in the NGRID data center.

SVG Program 2: Custom API for DOM manipulation

```
var newX1 = 50;
var newY1 = 50;
var redColour = "#FF0000";
NGRIDsvg.select("line001")
    .attr("x1", newX1)
    .attr("y1", newY1);
    .attr("stroke", redColour);
```

Original SVG is:

```
<svg width="500" height="500" xmlns="http://www.w3.org/2000/svg">
    <line id="line001" x1="0"   y1="0"
                       x2="400" y2="200"
          stroke-dasharray="2,2" stroke-width="1.0"
          stroke="#000000" />
</svg>
```

As mentioned in Table 1, the NGRID Test Application renders the patterns for the patient to do the VD tests. NGRID uses an embedded web browser in headless mode. This allows the same tests to be seamlessly used in any commodity hardware as-is and without any modification. SVG patterns are embedded inside the HTML5 canvas, which is controlled using the static test JavaScript APIs. These APIs allow for manipulation of the test graphics (i.e., showing the next pattern upon receiving the patient's answer) and automatically uploading the test results, answers and UI related events back to the NGRID database in the data center.

The NGRID Editor can be used to create a series of frames, to create or modify a VD test, and to save it in the NGRID library. Fig. 8, shows the NGRID customized SVG Editor, which allows NGRID designers to easily create various graphics for a frame or add additional frames to a test. Once the design process is done, by pressing the save button, all the frames will be stored in the NGRID database for later use. It is noteworthy to mention that SVG editing can be very complex as the graphics are expressed in mathematical vector notation. As aforementioned, the NGRID SVG Editor simplifies the SVG editing task by introducing very simplified features similar to Microsoft Paint.

4.4. Speech recognition and data collection during a VD test

Voice recognition is carried out via the NGRID voice recognition

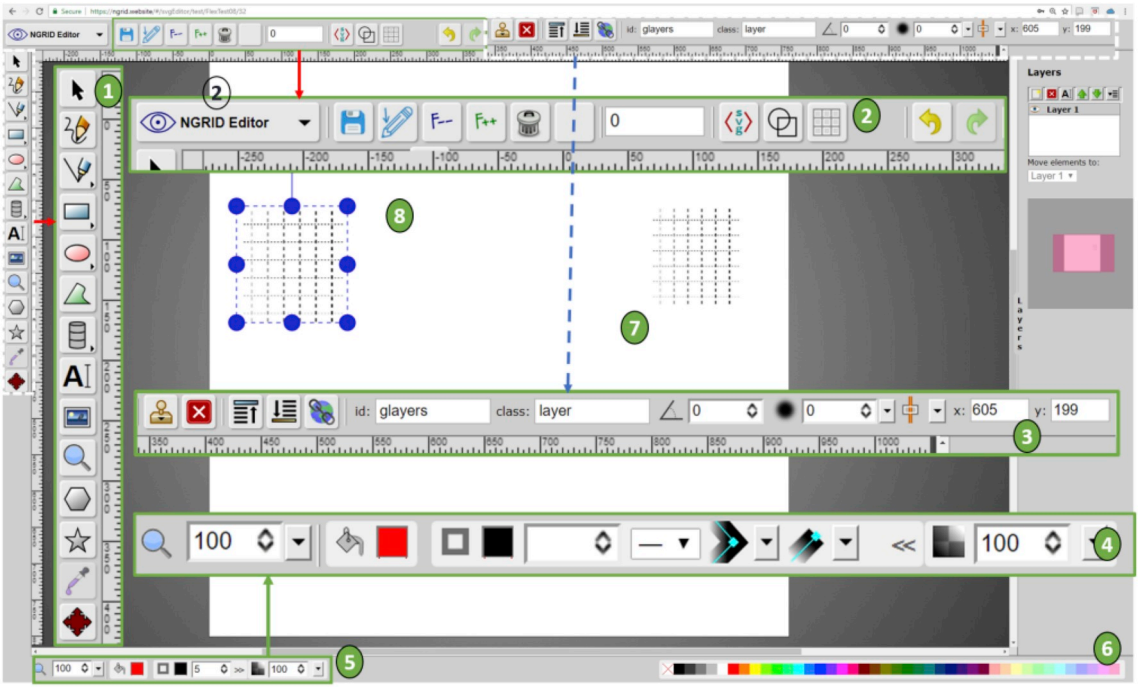

Fig. 8. NGRID Editor is a customized online SVG Editor for easy creation of VD test patterns. (1) Identifies the general editing buttons that allow for SVG pattern creation and modification (2) identifies the customized buttons that allow the automatic retrieval of the patterns from the NGRID data center. This allows for test data to be automatically mounted in the editor for editing purposes (3 and 4) are more detailed SVG editing tools that further allows the editor to rotate, group in layers or even change the style of the SVG patterns (5 and 6) are tools that are used to introduce various colours and opacities. (7 and 8) are sample VD patterns that are used to create the VD test frame.

engine which communicates the recognized voice phrases back to the visual distortion test through a secure web socket. Also, this engine logs in the detected words and/or commands. This communication between the sensory system and data collection is performed at a high-level. The NGRID speech recognition is first configured by setting up the local culture, the lexicon of detectable grammar words, amount of noise/silence required after each spoken word (here 200 m s) along with links to already established secure web-socket and database connections. Once the NGRID speech engine detects a word and/or command, it will store the results in a temporarily NoSQL DB Speech Log Table and also notify the client's VD test code, via a web-socket, about the recognized word. The client code will later act based on the state of the test and the recognized speech.

Each test has a specific lexicon that is accepted by the NGRID speech recognition engine via a file called ngrid. speech. The content of ngrid. speech can be modified by test designers. In this work, we used the following words 'Yes', 'No', 'Bad', 'Brighter', 'Darker', 'Finish', 'Good', 'Next', 'Pause', 'Previous', 'Stop', 'Thicker', 'Thinner' and 'Wait' to control various aspects of our NGRID VD tests. Using only one-word voice commands that we predefined in our lexicon (in contrast to complex natural language processing), allowed us to achieve faster and more accurate speech recognition. The program snippet below (see SVG Program 3) provides a high-level instantiation of the NGRID's speech engine.

4.5. NGRID administrative user interface

NGRID Admin is a series of online admin user interfaces (UIs) which were designed for patient data entry and test control purposes. The general admin UI was designed for adding patients' information, and the control admin UI was designed for controlling the VD tests. The NGRID admin interfaces are written in Scala in order to benefit from the load balancing done at the hardware level to serve many concurrent connections, thus allowing it to serve many hospitals and patients. It also uses a caching layer to save the most frequently used queries or VD tests to enhance further the speed of serving patients and medical practitioners.

General Admin: To perform a VD test for a patient, first, the patient should be added to the system. Fig. 9 shows the process of adding a patient to the system. Importantly, the system does not retain any Electronic Health Records (EHR) of the patients. NGRID can provide a cross-reference ID to correlate patient test results to the hospital EHR. This approach assures one-way access of the EHR record to be initiated by the hospital's authorized personnel and further guarantees that any patient information is used or saved in the NGRID database. If sufficient authorization and consent are provided by both hospitals and patients (mainly for the patient's first name, last name, age, and gender), NGRID

SVG Program 3: Voice Recognition's Communication

```
NgridSpeechRecognitionEngine speech = new NgridSpeechRecognitionEngine("en-US");
speech.loadGrammar("ngrid.speech");
speech.endOfWord = 200; //ms
speech.speechRecognized += new AsyncEventHandler<EventArgs>(SpeechRecognized);
speech.storageDB = ngridNoSQLSpeechStorageDB;
speech.webSocketServerPipe = ws;

public SpeechRecognized(EventArgs e){
    storageDB.log(e.recognized.timestamp, paitentId, trialId, e.recognized.text);
    if (ws)
        ws.notify(e.recognized.timestamp, paitentId, trialId, e.recognized.text);
}
```

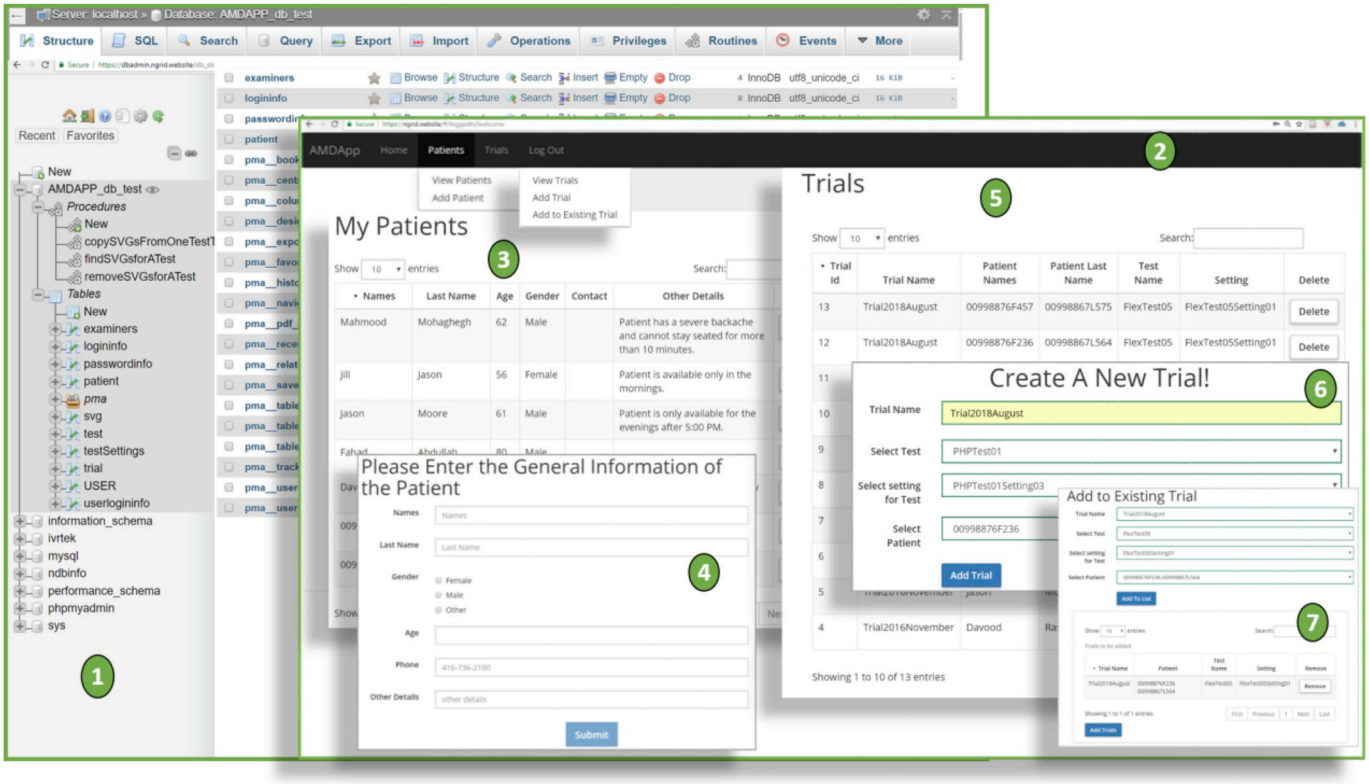

Fig. 9. (1) Specialized Database Admin Portal that allows for low-level archival and backup tasks to be done on the NGRID DB as well as an optimization on DB indices. (2) is the overview of the NGRID Admin interface that allows adding patients and assigning them to trials. (3,4) refer to how patients are added to the system. (5,6) refer to how a new trial is added to the system. (7) is used for how patients are assigned to trials.

can also retain this limited information. Once the patients are added to the system and the desired tests are created, an ID is generated and used instead of the actual personal information of the patient. The ID is unique and helps to keep the patient anonymous and also hides the associated clinical test details.

NGRID technical admin staff (or SVG VD test designer, see Fig. 8) also have direct access to the Test SVG Database Admin Interface (Fig. 9(1)) that allows them to perform various low-level DB Table archival and backups for the database. Fig. 9(2)-9 (7) show the NGRID General Admin interface (intended to be used by medical staff tasked with creating trials, adding patients to the system and assigning them to the trials). Fig. 10 shows the NGRID Control Test Admin interface (intended to be used by technical staff who implement the tests and run various low-level tasks and queries against the VD Test SVG tables).

Control Test Admin: This interface provides an easy way of manipulation and low-level manual configuration editing of SVGs for a VD test (see Fig. 10). The creation and modification of tests are mainly targeted for use by NGRID technical staff that are supervised by a participating doctor's office to create different VD test styles as per the request of the medical practitioner and ophthalmologists. Fig. 10, shows the Control Test Admin interface that allows for adding new staff to the system as well as creating and customizing new NGRID VD Tests. It is noteworthy that patients can benefit from NGRID with a preset of built-in tests as well as more specialized customized tests are created based on the ophthalmologists' instructions. New tests can be added and edited via the online SVG Editor, as explained in subsection IV-C.

4.6. NGRID heatmap

As mentioned in Table 1, the NGRID Heatmap Generator program is developed to create a diagram with quantitative measures of the damaged VD area. It aims to both visually and quantitively measure the damaged area in the retina. As aforementioned, NGRID VD tests show a series of graphical patterns to the patients and collect their answers. The answers are post-processed in the NGRID datacenter that later is used by the NGRID Heatmap Generator program to render a visualized heatmap along with the Heat-index score. The NGRID heatmap generator program finds the location of the scotoma and metamorphopsia by going through patients answers frame-by-frame to create Perfect-Matrix (PM) and HeatMatrix (HM). PM uses rasterized graphics from SVGs by considering the display resolution and pixel density at which the test is performed. HM will be similar while it distinguishes the frames that are seen as 'Bad' or '1s' (e.g., due to the presence of metamorphopsia or scotoma). The HeatMap Matrix (HMM) is calculated by using HMM = PM – HM. This matrix provides the location of VDs along with the severity of the VDs at each location. Let us assume, F(i) is a matrix representing a frame from a series of N frames that are sequentially projected on the retina where $0 < i < N+1$ and F(i) is an $m \times m$ matrix that represents an $m \times m$ image. N and m are natural numbers. In the following example, N = 16 and m = 5, however in the actual VD tests, m and N can be much higher (e.g., m = 800 pixels and N = 167). In this example, the sixteen frames were defined with different patterns as seen in Fig. 11.

Each frame can be represented with one of the following matrices F (1)–F (16).

$$F(1) = \begin{bmatrix} 1 & 1 & 1 & 1 & 1 \\ 0 & 0 & 0 & 0 & 0 \\ 0 & 0 & 0 & 0 & 0 \\ 0 & 0 & 0 & 0 & 0 \\ 0 & 0 & 0 & 0 & 0 \end{bmatrix}, F(2)$$

$$= \begin{bmatrix} 0 & 0 & 0 & 0 & 1 \\ 0 & 0 & 0 & 0 & 1 \\ 0 & 0 & 0 & 0 & 1 \\ 0 & 0 & 0 & 0 & 1 \\ 0 & 0 & 0 & 0 & 1 \end{bmatrix}, F(3) \begin{bmatrix} 0 & 0 & 0 & 0 & 0 \\ 0 & 0 & 0 & 0 & 0 \\ 0 & 0 & 0 & 0 & 0 \\ 0 & 0 & 0 & 0 & 0 \\ 1 & 1 & 1 & 1 & 1 \end{bmatrix}, F(4) \begin{bmatrix} 1 & 0 & 0 & 0 & 0 \\ 1 & 0 & 0 & 0 & 0 \\ 1 & 0 & 0 & 0 & 0 \\ 1 & 0 & 0 & 0 & 0 \\ 1 & 0 & 0 & 0 & 0 \end{bmatrix},$$

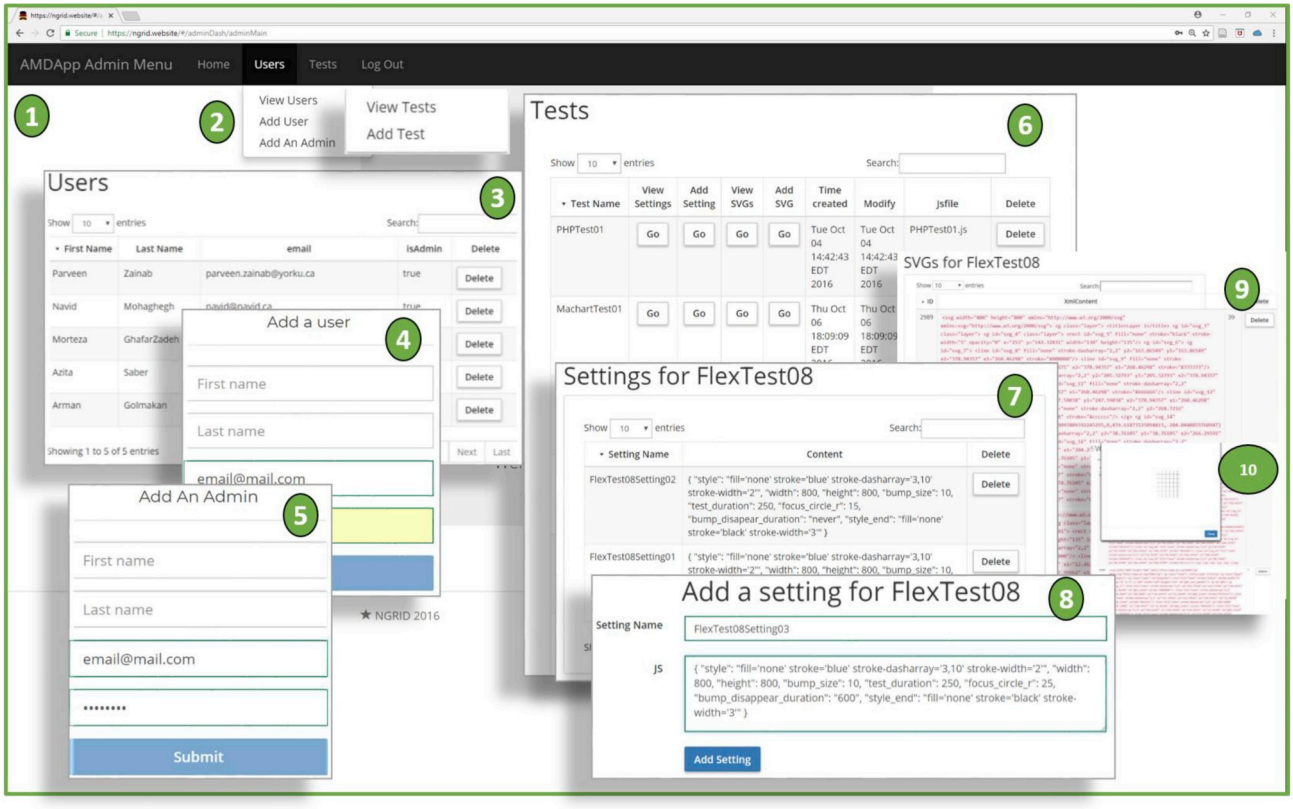

Fig. 10. Control Test Admin UI: (1) the overall online interface that allows staff and admins to be added to the system as well as creating and editing new NGRID VD Tests. (2,3,4,5) allows for adding new staff (medical practitioner) and admins (NGRID test designers and technical staff) to the system where only names, the email address is required. (6) shows the existing library of VD tests in the system. (7,8) the medical practitioner can administer the test once the VD test is designed and stored in NGRID library by adding a new test with customized settings. (9,10) A test needs a name, series of settings such as duration of a test and for advance animated test associated scripts, low-level modification to SVG codes associated with a test. This is where the NGRID SVG Editor is launched, as shown in Fig. 8.

$$F(5)=\begin{bmatrix}0&0&0&0&0\\0&1&1&1&0\\0&1&1&1&0\\0&1&1&1&0\\0&0&0&0&0\end{bmatrix},F(6)=\begin{bmatrix}0&0&0&0&0\\1&1&1&1&1\\0&0&0&0&0\\0&0&0&0&0\\0&0&0&0&0\end{bmatrix},F(7)$$
$$=\begin{bmatrix}0&0&0&0&0\\0&0&0&0&0\\1&1&1&1&1\\0&0&0&0&0\\0&0&0&0&0\end{bmatrix},F(8)=\begin{bmatrix}0&0&0&0&0\\0&0&0&0&0\\0&0&0&0&0\\1&1&1&1&1\\0&0&0&0&0\end{bmatrix},$$

$$F(9)=\begin{bmatrix}0&1&0&0&0\\0&1&0&0&0\\0&1&0&0&0\\0&1&0&0&0\\0&1&0&0&0\end{bmatrix},F(10)=\begin{bmatrix}0&0&1&0&0\\0&0&1&0&0\\0&0&1&0&0\\0&0&1&0&0\\0&0&1&0&0\end{bmatrix},F(11)$$
$$=\begin{bmatrix}0&0&0&1&0\\0&0&0&1&0\\0&0&0&1&0\\0&0&0&1&0\\0&0&0&1&0\end{bmatrix},F(12)=\begin{bmatrix}0&0&0&0&1\\0&0&0&1&0\\0&0&1&0&0\\0&1&0&0&0\\1&0&0&0&0\end{bmatrix},$$

$$F(13)=\begin{bmatrix}1&0&0&0&0\\0&1&0&0&0\\0&0&1&0&0\\0&0&0&1&0\\0&0&0&0&1\end{bmatrix},F(14)=\begin{bmatrix}1&1&1&1&1\\1&1&1&1&1\\0&0&0&0&0\\0&0&0&0&0\\0&0&0&0&0\end{bmatrix},F(15)$$
$$=\begin{bmatrix}0&0&0&0&0\\1&1&0&1&1\\1&1&0&1&1\\1&1&0&1&1\\1&1&0&1&1\end{bmatrix},F(16)=\begin{bmatrix}1&1&0&1&1\\1&1&0&1&1\\1&1&0&1&1\\1&1&0&1&1\\1&1&0&1&1\end{bmatrix}$$

Let us assume that the answer of a patient to each frame F(i) can be represented with AN(i) where $0 < i < 17$. More precisely $A(i) = 0$ when the answer is 'good' and $AN(i) = 1$ when the answer is 'bad.' In this example, the AN matrix is equal to [0 0 1 0 1 0 1 1 0 1 0 1 1 0 0 0].

The combination of all frames results in a PM that can be obtained from the following equation. For our sample frames (F (1)–F (16)) the value of PM is shown in Equation (2).

$$PM=\sum_{i=1}^{i=16}F(i) \tag{1}$$

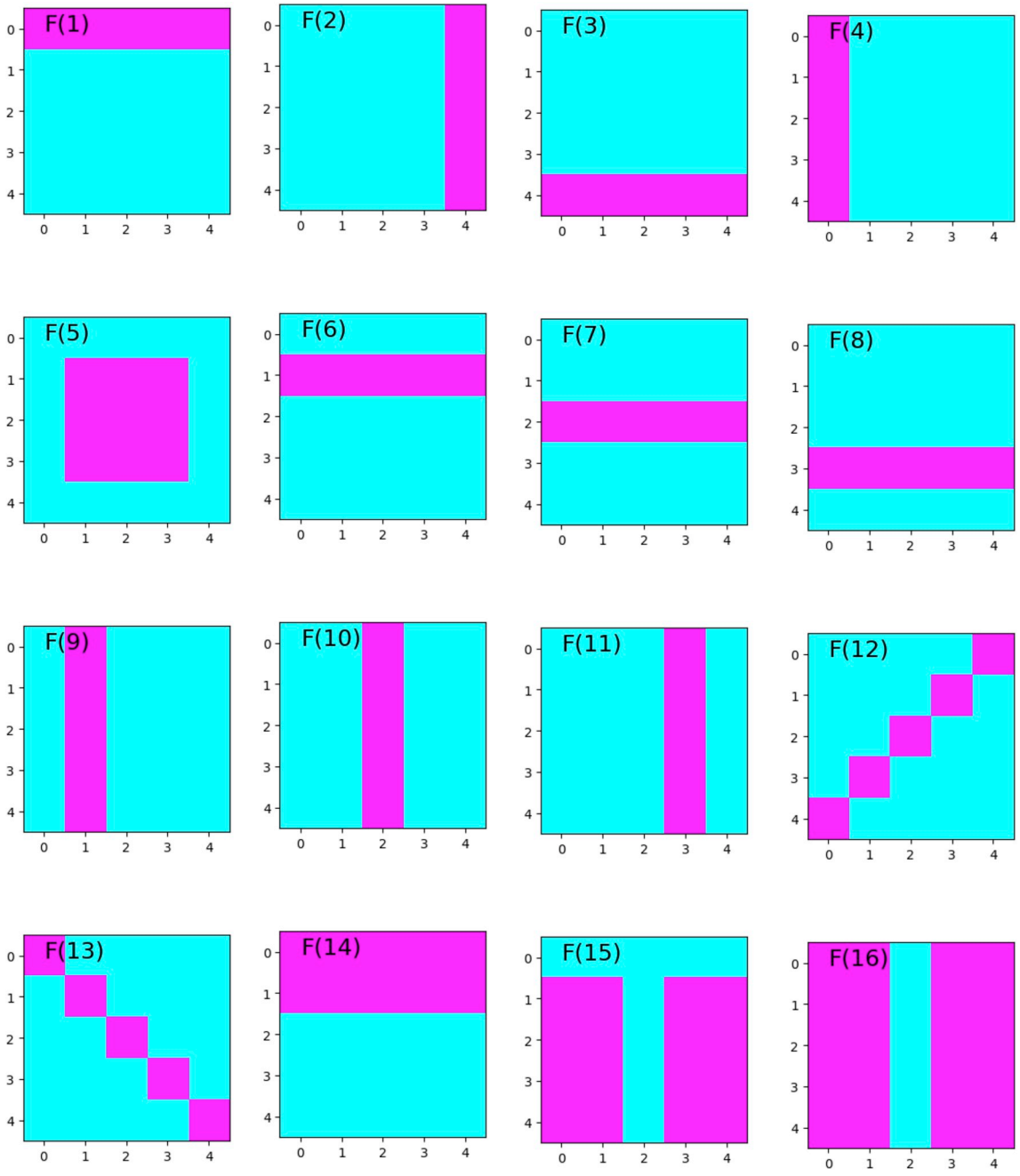

Fig. 11. An example of 16 frames in a simplified demonstration of the heatmap algorithm.

$$PM = \begin{bmatrix} 5. & 4. & 3. & 4. & 5. \\ 5. & 7. & 4. & 7. & 5. \\ 4. & 5. & 5. & 5. & 1. \\ 5. & 6. & 3. & 6. & 4. \\ 5. & 4. & 2. & 4. & 5. \end{bmatrix} \quad (2)$$

The PM matrix is also used as the initial value of the heat matrix (HM). We now start sifting through the patient's answers. In this example, for frame $0 < i < 17$, if AN(i) is 'good', then equation (3) is obtained and if AN(i) is 'bad', then equation (4) will be obtained.

$$HM = HM + F(i) \quad (3)$$

$$HM = HM - k * F(i) \quad (4)$$

where $k = 2$ is used in this experiment. Therefore, the obtained HM is as follows

$$HM = \begin{bmatrix} 7. & 8. & 3. & 0. & 7. \\ 10. & 8. & 2. & 8. & 10. \\ 5. & 4. & -5. & 4. & 5. \\ 5. & 3. & -3. & 3. & 5. \\ 4. & 5. & -2. & 5. & 4. \end{bmatrix} \quad (5)$$

By differentiating PM and HM, HMM (HMM = PM – HM) is obtained as follows

$$HMM = \begin{bmatrix} -2. & -4. & 0. & -4. & -2. \\ -5. & -1. & 2. & -1. & -5. \\ -1. & 1. & 10. & 1. & -1. \\ -1. & 3. & 6. & 3. & -1. \\ 1. & -1. & 4. & -1. & 1. \end{bmatrix} \quad (6)$$

All values lower than the mean values of $\overline{\overline{HMM}} = \sum_{i=1}^{i=5} \sum_{j=1}^{j=5} \frac{HMM(i,j)}{25}$, which is zero in this example, will be ignored. Thus, the new HMM is obtained as follows

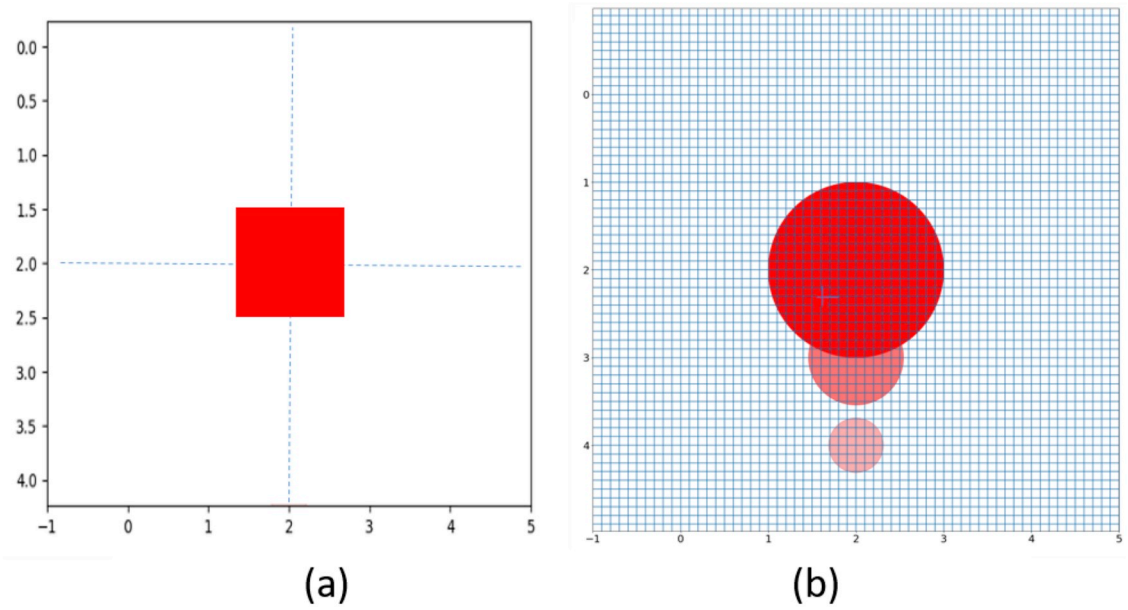

Fig. 12. An example of creating heatmap: (a) two overlapped features and (b) single, larger feature covering the second part.

$$HMM = \begin{bmatrix} 0 & 0 & 0 & 0 & 0 \\ 0 & 0 & 2 & 0 & 0 \\ 0 & 1 & 10 & 1 & 0 \\ 0 & 3 & 6 & 3 & 0 \\ 1 & 0 & 4 & 0 & 1 \end{bmatrix} \quad (7)$$

It is noteworthy that in equation (4), instead of -2F(i), -kF(i) can be used where $k > 2$. By increasing k, the heatmap can better distinguish the locations with VDs from the rest of the visual field. The z-score of the HMM values are obtained as seen below using the $z = (X - \mu)/\sigma$ relationship, where z is the z-score, X is the value of the element, μ is the population mean, and σ is the standard deviation (SD). This can further differentiate values according to SD lower than μ. It is noteworthy that, using the Z-score and other functions below, the pixels involved in the VD area are differentiated from other pixels. This process will result in increasing the visibility of the NGRID heatmap even if the frames processed are minimal (in real VD tests a much higher number of frames are displayed).

$$HMM_Z = \begin{bmatrix} -0.5467091 & -0.5467091 & -0.5467091 & -0.5467091 & -0.5467091 \\ -0.5467091 & -0.5467091 & 0.30752387 & -0.5467091 & -0.5467091 \\ -0.5467091 & -0.11959261 & 3.72445571 & -0.11959261 & -0.5467091 \\ -0.5467091 & 0.73464035 & 2.01598979 & 0.73464035 & -0.5467091 \\ -0.11959261 & -0.5467091 & 1.16175683 & -0.5467091 & -0.11959261 \end{bmatrix} \quad (8)$$

By clamping on the heatmap z-score values higher than 75% of SD, the following matrix clamped Z-score HMM_{ZC} may be obtained.

$$HMM_{ZC} = \begin{bmatrix} 0 & 0 & 0.00 & 0 & 0 \\ 0 & 0 & 0.00 & 0 & 0 \\ 0 & 0 & 3.72 & 0 & 0 \\ 0 & 0 & 2.01 & 0 & 0 \\ 0 & 0 & 1.16 & 0 & 0 \end{bmatrix} \quad (9)$$

For the selection of this threshold, a simple experimental process has been employed. Using the same NGRID test results as introduced above, we observe heatmaps with different thresholds. The lower the threshold, the larger the number of VDs, likely with less accuracy, that can be observed in the visual field. This matrix can be converted to a heatmap pattern, as seen in the heatmap (Fig. 12b). The heatmap figure indicates the visual field with visual distortion. As aforementioned, in each pixel, a circle with a certain opacity is drawn. The opacity (OP) and radius (RA) matrices are obtained as discussed below.

$OP = 100*HMM_{ZC}/Max\ (HMM_{ZC})$ where each member of OP is between 0 and 100 and "Max" is a function that finds the maximum value in the matrix. The lower the value in the OP, the higher the transparency will be at the heatmap circle drawn at that location. The colour of each circle in each pixel is obtained from the following matrix.

$$OP = \begin{bmatrix} 0 & 0 & 0.00 & 0 & 0 \\ 0 & 0 & 0.00 & 0 & 0 \\ 0 & 0 & 100 & 0 & 0 \\ 0 & 0 & 54.1 & 0 & 0 \\ 0 & 0 & 31.2 & 0 & 0 \end{bmatrix} \quad (10)$$

Similarly, the radius matrix (RA) is obtained so that $RA = k*HMM_{ZC}/Max\ (HMM_{ZC})$ where each member of RA is between 0 to k (k is defined in each VD test and can be set from 1 to 20 depending on the sparse area of the combined collapsed frames). It is noteworthy that k tries to factor in the area that no graphical coverage is done in the VD test. Herein we select $k = 1$. The lower the value in RA, the smaller than the radius of the circle will be. The radius of the corresponding heat location will be:

$$RA = \begin{bmatrix} 0 & 0 & 0.00 & 0 & 0 \\ 0 & 0 & 0.00 & 0 & 0 \\ 0 & 0 & 1 & 0 & 0 \\ 0 & 0 & 0.54 & 0 & 0 \\ 0 & 0 & 0.31 & 0 & 0 \end{bmatrix} \quad (11)$$

It is also noteworthy that the values in the RA matrix cannot be directly rendered in the heatmap graphical canvas without scaling up the values according to the canvas resolution. The following RA matrix demonstrates the values of RA rounded-up to the nearest integer:

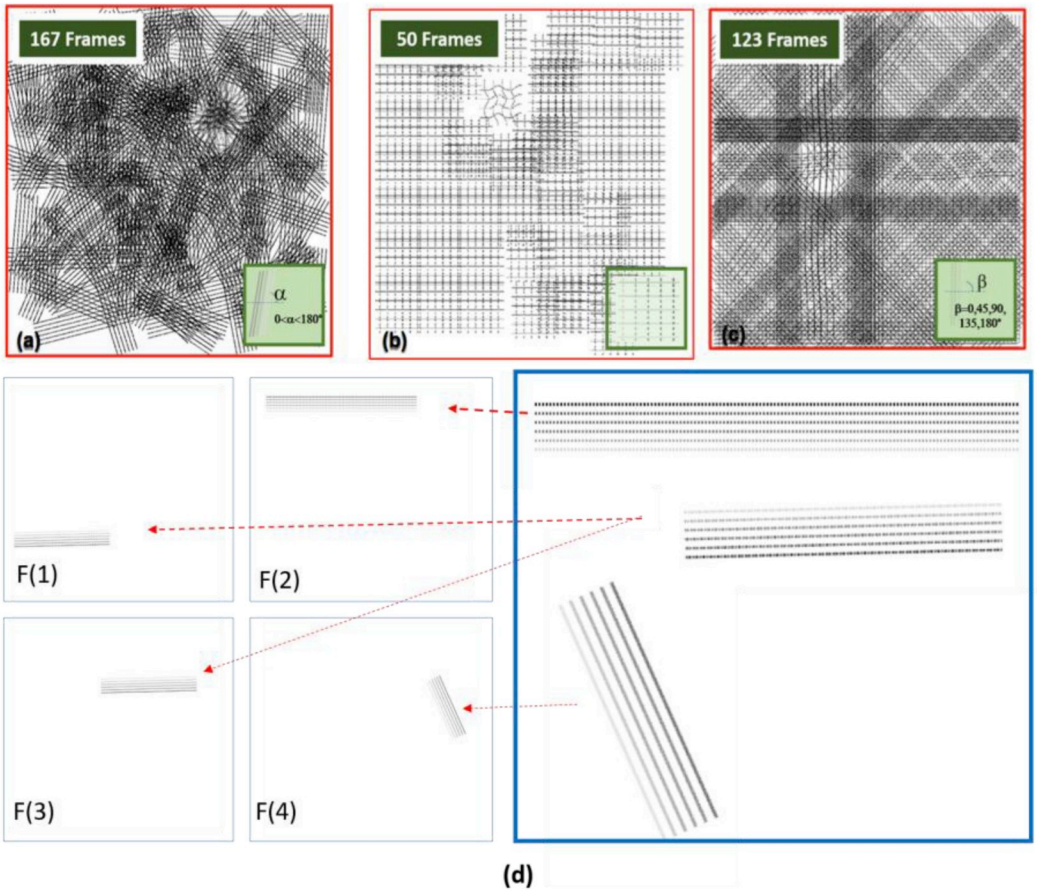

Fig. 13. Illustration of (a) VDT1, (b) VDT2 and (c) VDT3 including all frames collapsed in a single frame to better illustrate the entire test coverage; (d) four frames F (1)–F (4) of VDT1 test.

$$RA_r = \begin{bmatrix} 0 & 0 & 0 & 0 & 0 \\ 0 & 0 & 0 & 0 & 0 \\ 0 & 0 & 1 & 0 & 0 \\ 0 & 0 & 0 & 0 & 0 \\ 0 & 0 & 0 & 0 & 0 \end{bmatrix} \quad (12)$$

This matrix is called a rounded radius matrix (RA_r) as shown in Fig. 12a. In this approach, it is crucial to scale up the RA values based on the size of the drawing heatmap canvas. As demonstrated in Fig. 12b, the drawing heatmap canvas has a higher resolution with three heatmap circles.

RA and OP matrices define the radius and opacity of each heatmap circle. For instance, considering the above RA matrix, for $RA_{(3,4)} = 0.54$ to be drawn in a heatmap canvas of size 400 × 400 pixels, will result in a scaled-up factor of 80 (e.g., 5 × 5 to 400 × 400). This means values for drawing a circle at pixel location (3,4) are mapped to (240, 320) with a radius of 43 pixels (location of $3 \times 80 = 240$ and four × 80 = 320 as well as a radius size of $0.54 \times 80 = 43.2$ pixels which rounded to 43 pixels).

As seen in Fig. 12b, the heatmap area is highlighted and shows where the patient experiences VD. The percentage of the VD area in the visual field (η) and the center of this area (χ) can be calculated as follows. To obtain η, a program was developed to count the total number of pixels under the heatmap area. In this example (Fig. 12b), η is calculated to be 11.25%.

To calculate the coordinates of χ, for each pixel in the heatmap area, RA_{ij} and OP_{ij} represent the opacity and relative radius in *i* and *j* Cartesian coordinates. By knowing that OP_{22} is 100% in (2, 2), using the following equations (13) and (14), the center of the heatmap area will be obtained (and scaled up in the drawing heat canvas accordingly) as follows.

$$x_\chi = Av(i * OP_{ij}) \quad (13)$$

$$y_\chi = Av(j * OP_{ij}) \quad (14)$$

where Av () represents a function that obtains the mean value of *i* and *j* for all available non-zero OP_{ij}. In this example, by substituting, (2, 2) and the related opacity in the above equations, χ will be equal to (2, 2) that will be scaled up to pixel coordinates of (160,160) in the drawing canvas size of 400 × 400 pixels. It is noteworthy that we can use a larger drawing canvas in order to show heatmap with higher accuracy for medical purposes. Here we demonstrate a scale-up factor of 80 (e.g., 400 × 400 pixels from 5 × 5 pixels) while in our real VD tests we start with a minimum of 800 × 800 as well as 1200 × 1200. It is noteworthy that we can further improve the accuracy of the estimated center of damage and other geometries shown in the heatmap using floating-point instead of integer numbers.

In the next section, we discuss the results and present the heatmap of VDs that are generated using the outlined NGRID Heatmap Generator program.

5. Results

In this section, we demonstrate and discuss the experimental results using healthy and non-healthy human participants.

5.1. NGRID test on healthy participant

As shown in Fig. 13, three different VD tests (VDT1, VDT2, and VDT3) from the NGRID default library were selected. Three different control input devices (keyboard, joystick, and speech recognition) for

Table 2
General tests specification.

Test	Duration (seconds)	Number of Frames	Average and Standard Deviation of Errors	Average and Standard Deviation of Response Times (seconds)
VDT1	480	167	8.3% ± 4.2%	1.16 ± 0.45 s
VDT2	180	50	15.6% ± 20.7%	0.97 ± 0.48 s
VDT3	360	123	9.1% ± 5.5%	1.03 ± 0.42 s

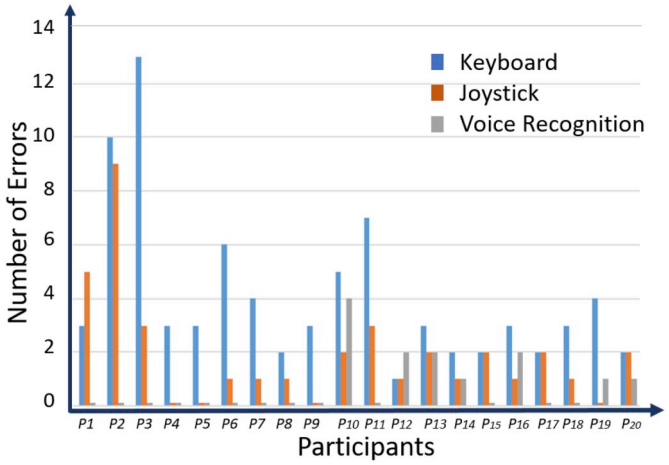

Fig. 14. Systematic error in VD tests performed by healthy participants based on a control device.

each test were also selected. Twenty healthy participants (12 females, eight males) with healthy corrected vision were recruited from the local university to test the NGRID platform. The mean age was 23.8 years (SD = 6.1). The healthy participants were selected to identify inherited systematic errors and any accuracy issues of the platform. Each participant was trained for 10 min and instructed to each VD test with all the control input devices using counterbalance of above tests and devices (3 VD Tests × 3 Input Devices). The apparatus was the same as that shown in Fig. 5. A chin rest was used to assure that the participants could comfortably fixate at the center of the screen.

Visual Tests' Frames: As described in section II, we used the customized SVG Editor to create three VD tests. VDT1 is composed of a total of 167 frames that were individually presented to the participants in random order. Similarly, we have 50 frames for VDT2 and 123 frames for VDT3. For illustration purposes, and to better explain the procedure, in Fig. 13, we intentionally collapsed all the frames into a single frame for clearer visualization. Since we measured systematic errors in the system (by having healthy participants), we deliberately added a few distorted patterns in the tests to assure participants carefully go through the test without being able to predict answers (otherwise they could say they saw all the frames as 'Good'). As seen in Fig. 13d, each frame of VDT1 contains a pattern which includes several lines with different styles.

As seen in Fig. 13, the projected frames cover the entire screen, which spans the central 20° of the field of view in both horizontal and vertical lines (nasal projection). As seen in Fig. 13b, VDT2 is very similar to VDT1, with the difference in the rotation angle (β) being 45°κ (where κ is an integer number between 0 and 8). VDT2 also includes a single distorted pattern similar to distorted patterns in VDT1. VDT3 is composed of parallel lines (patterns are presented in Fig. 13c). VDT3 patterns are displayed with a random rotation angle (α) ranging from 0° to 360°. It is noteworthy that the lack of patterns related to the edges of the screen shown in Fig. 13b does not cause any problem for the detection of a macular disorder.

VD Test Procedure: In this work, for the characterization of the proposed NGRID platform as well as evaluating the errors and response times, we used the VDT1 above, VDT2, and VDT3. Each participant

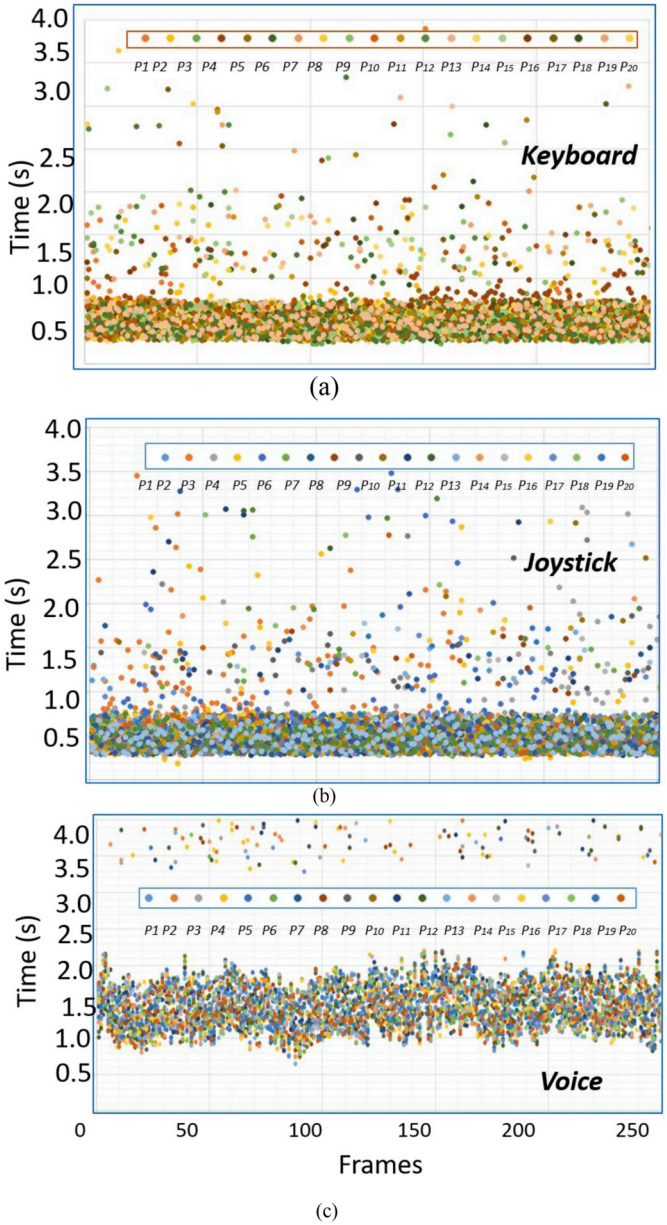

Fig. 15. The response time diagram related to control input devices (a) Keyboard, (b) Joystick, and (c) Voice recognition used for performing VD tests. The voice recognition has the longest response times whereas the keyboard and joystick produced the shortest.

repeated the same three tests three times using different control devices (e.g., keyboard, joystick, and voice recognition). For the keyboard, participants were asked to press the 'G' key to indicate the absence of VD and 'B' to indicate a positive response to the presence of VD. Similarly, on the joystick, two buttons were marked as 'G' and 'B'. For voice recognition, users could simply say 'Good' or 'Bad' when they observed distorted or non-distorted patterns. The number of frames and the time duration of each test are shown in Table 2. The higher the

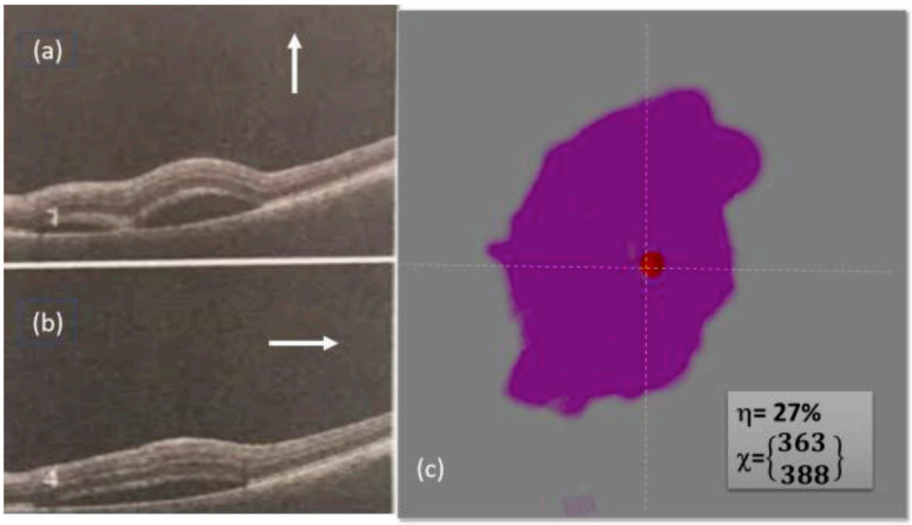

Fig. 16. First Macular Disorder Measurement Results of left Eye: (a)–(b) OCT vertical and horizontal OCT images and (c) NGRID heatmap results with η = 27% and χ = (363, 388).

number of frames, the longer the test duration that was dedicated. It seems the error in VDT1 is less than others. This might be because VDT2 and VDT3 repeat similar shapes in different locations. Therefore, the participants did not pay sufficient attention to provide answers accurately; however, in VDT1 there are no two similar patterns.

Experimental Results: The VD tests were performed by all healthy participants. Fig. 14 shows the number of wrong responses (here referred to as errors) where the patterns with straight or distorted lines are displayed to the patients. Indeed, the patterns with distorted lines artificially induced VDs to healthy human subjects. The correct responses should be '1' and '0' where the patterns include or don't include VDs, respectively. Otherwise, the response is wrong. Fig. 15 shows the response time for VDT1, VDT2, and VDT3. The mean values of errors and response times are shown in Table 2. It is noteworthy that information related to errors and response times were extracted from the detailed log of captured responses during the test. The log provides detailed recording of speech, keyboard and joystick actions as well as the time of each event in milliseconds. Please refer to previous sections for details of the apparatus.

As seen in Fig. 14, the errors made by each one of the twenty healthy participants combined in all three VDT1, VDT2 and VDT3 tests separated by the control device (joystick, keyboard, and voice) are presented. For this purpose, we extracted and analyzed the responses associated with each one of the control devices separately from the logs. Speech recognition had the least number of errors as a participant could effortlessly say what they think about a frame seen, and no pointing task was involved. Participants made the maximum number of errors when they used the keyboard and made the minimum number of wrong responses when they used voice recognition. One may argue that participants have to pay attention to press the right keys in the keyboard and carefully fixate at the center of the display. In agreement with the experimental results, this increases the number of systematic errors. The joystick with less need for visual attention can be used, which is in conformance with the presented experimental results. As expected, the participants, while looking at the center of the display, could speak their responses without losing their attention or fixation point. This is why the errors made by participants when they use voice recognition device were lower than the errors made using the other two control input devices.

It is noteworthy that VDT2 had only one artificially induced VD across all the frames. We noticed a high number of errors (as high as 35%) on this particular test. We also noticed that many participants expressed frustration for missing the one artificially induced VD while doing the test. This can be considered as a systematic error that can be easily avoided by changing the colour or shape of the patterns to make it less similar to other patterns. Another unlikely, but possible, the hypothesis was that some of the participants could suffer from a minor macular disorder. However, these participants were able to identify the distorted pattern in VDT1 and VDT3 successfully. As aforementioned, we think that since the patterns in VDT2 were very similar to each other and that there was only one artificially induced VD created, coupled with the fact that participants wanted to finish the test as fast as possible, caused this systematic error in VDT2. As per the results are shown in Fig. 14, the voice recognition system offers higher accuracy in comparison with the results shown in the same figure related to the keyboard and joystick input devices. It seems the latter input devices shift the concentration and fixation of patients from watching the display to touching the device.

As mentioned, Fig. 15*a-c* shows the response times for each frame captured for twenty participants using the keyboard, joysticks and voice recognition system, respectively. In this result, the combination of three different VD tests performed by all twenty participants was used where each participant is distinguished with a certain colour in the result charts. Each participant had a fixed time to do the test and, depending on their speed, could go through all the frames a few times. Voice recognition, in comparison to the joystick and keyboard, demonstrates a slower control device. One may argue that this depends on the speed of the voice recognition system, therefore using a real-time digital system, it may be possible to reduce the response time. However, we also need to remember that speaking a simple single word like 'Good' or 'Bad' will take more time compared to a simple binary pointing task such as pressing a button [27]. As expected, the response time when the participants used the keyboard or joystick was almost the same.

It is noteworthy that the response time in each frame has three components. These components are (a) the required time that participant needs to make a decision about a frame just seen and (b) the required time that a participant needs to react and take action using the control input device and (c) the required time that the computer needs to process the response received from the participant. We assumed the first component is almost the same when different control devices are used.

5.2. NGRID test on non-healthy participant

In this sub-section, we demonstrate and discuss the functionality and applicability of the proposed interface system for non-healthy

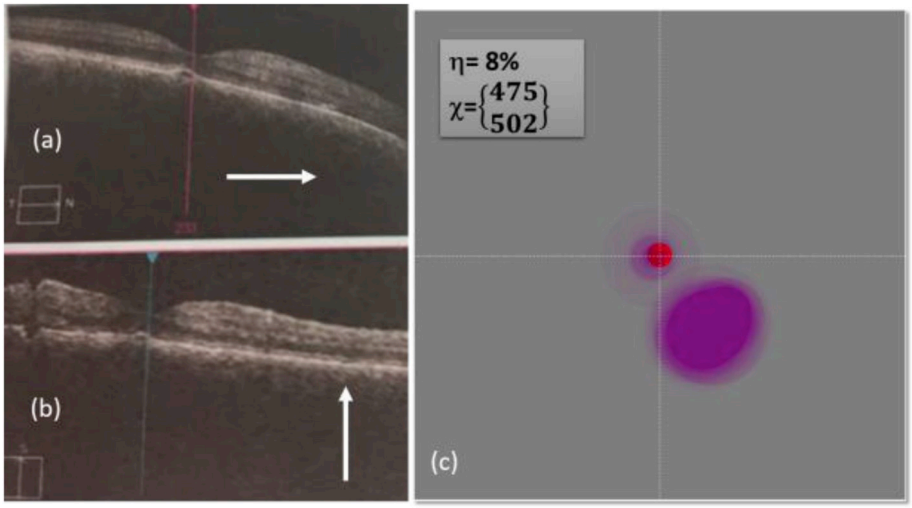

Fig. 17. First Macular Disorder Measurement Results of right Eye: (a)–(b) OCT vertical and horizontal OCT images and (c) NGRID heatmap results with $\eta = 8\%$ and $\chi = (475, 502)$.

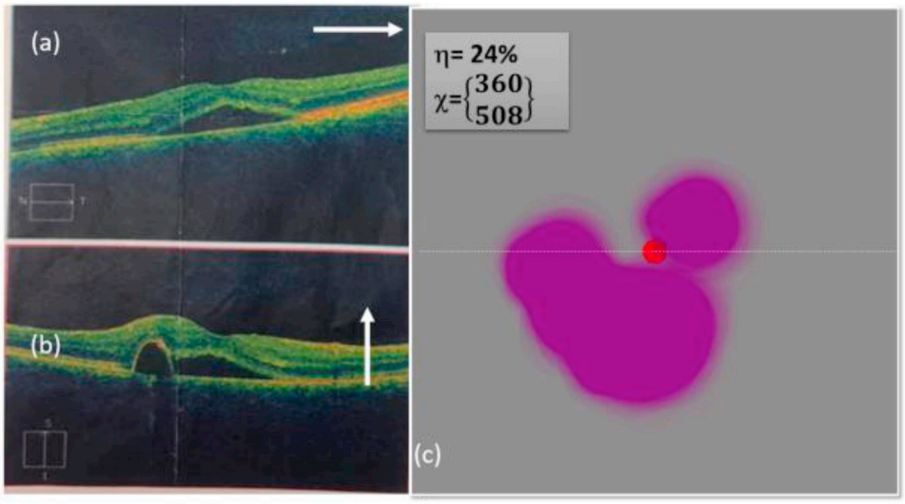

Fig. 18. - Second Macular Disorder Measurement Results of left Eye: (a)–(b) OCT vertical and horizontal OCT images and (c) NGRID heatmap results with $\eta = 24\%$ and $\chi = (360, 508)$.

participants suffering from a macular condition called Central Serous Chorioretinopathy (CSCR or CSR) [2].

Central Serous Chorioretinopathy is an idiopathic macular condition and usually happens in men aged between 20 and 50 (10 annual cases in 100,000 males) [28], but is also associated with high levels of stress and usage of inhaled steroids [28,29]. Studies show disturbing psychological events and high levels of stress can trigger CSR in more than 75% of the patients [30]. Also, some studies link sleep disturbances, hypertension, and autoimmune diseases to CSR [28,29]. For diagnosis purposes, an eye-care professional starts examining a dilated eye and performs optical coherence tomography (OCT) and fluorescein angiography. This may reveal localized serous detachment of the neurosensory retina at the level of retinal pigment epithelium (RPE). The Amsler Grid is used for documenting the affected areas of the visual field. Most of the patients are expected to have a full recovery between one and six months. In rare chronic cases, laser treatment, photodynamic therapy, or even Ranibizumab Anti-VEGF are utilized (reduced visual acuity may persist) [3,31]. CSR can become a recurrent problem, which makes follow-ups necessary [3].

Optical Coherence Tomography: OCT is a non-invasive medical imaging technique used to provide optical cross sections of the retina [32]. It is based on low-coherence interferometry, employing near-infrared light. It uses light to capture micrometre-resolution, three-dimensional images. These images are high resolution and allow changes in retinal thickness to be seen. OCT can play an important role in evaluating patients macular disorders [4,32].

NGRID and OCT Tests: In this sub-section, the results of the NGRID test and corresponding OCT images are demonstrated and discussed. We used the OCT images of a participant as the control of NGRID results. The subject is a 48-year-old male suffering from CSR. The rapid change of his macular condition allowed us to perform the NGRID tests on the same patient at three different times that resulted in completely different OCT images. Therefore, we have effectively tested three different cases (or three different macular deformations) on both left and right eyes separately. The subject performed the VD tests using VDT1, VDT2, and VDT3, but without being shown any distorted patterns. The responses for NGRID VD tests were collected, post-processed and heatmaps were generated through the NGRID Heatmap Generator program. Fig. 16 to Fig. 21 show the NGRID heatmaps and their corresponding OCT images. The experiments were performed on both eyes separately. NGRID detected VD on each eye, which fully conforms to OCT images. The heatmaps were generated using the NGRID Heatmap program by using the algorithm explained in Section IV-F. Based on the results shown in Figs. 16–21, the proposed NGRID platform can be used

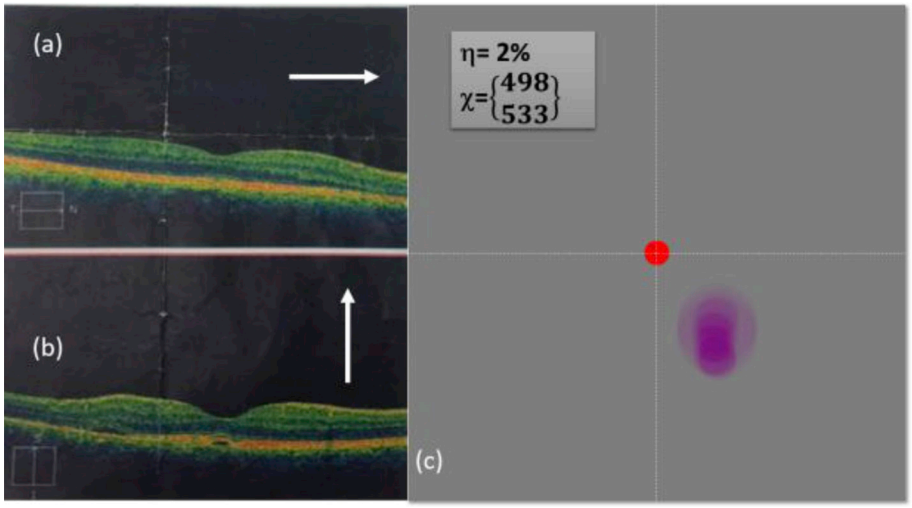

Fig. 19. Second Macular Disorder Measurement Results of right Eye: (a)–(b) OCT vertical and horizontal OCT images and (c) NGRID heatmap results with η = 2% and χ = (498, 533).

as an accurate method to detect and assess the progress of macular disorders.

The subject visited the Sunnybrook Hospital Emergency Room (ER) while observing a large yellow circle in the center of his vision. The subject also complained about metamorphopsia upon seeing the paper-based Amsler grid. AMD and CSR were the initial diagnoses based on the symptoms. However, OCT images from his left eye revealed a CSR macular condition. Fig. 16 shows the OCT images and related heatmap result.

As per this NGRID result in Fig. 16, the VD left eye of the patient is about 27%. The damage is almost placed in the center (363, 388) of the visual field where the exact center of the display is located at Cartesian coordinates x = 400 and y = 400. Fig. 16a–b (similarly for other Figs. 16–21), show the vertical and horizontal cross section of the retina. Fig. 16c (likewise for other Figs. 16–21), show the damaged area from the top. Fig. 17, shows the OCT images along with their corresponding NGRID heatmap images related to the right eye in the first visit. As seen in this figure, η = 8% and χ = (475, 502). Based on this result, the right eye also shows the CSR condition. However, the patient did not complain because the effect of CSR was negligible in his vision. Fig. 18 and Fig. 19 show the OCT and heatmap NGRID results related to left and right eyes, respectively, after a couple of weeks. As seen in these results, η has been decreased in both eyes. This shows that the CSR was reduced. However, in the third visit, the CSR in the left eye had not been decreased (approximately with the same η). In Fig. 20 and Fig. 21, both OCT and NGRID images show that the effect of CSR in the left and right eyes have been decreased respectively. It is noteworthy that the location of the CSR disorder in the retina can move from one spot to another. This is because the leading cause of CSR is the influence of fluid under the basement of the retina. This fluid can move over time due to eye movement and other activities. Based on the experimental results shown in Figs. 16–21, the NGRID heatmap's results are accurately in agreement with OCT results. The VD tests can be rapidly performed, and the heatmap results can be used to assess the progress of the macular disorder quantitatively.

6. Conclusion

In this paper, we proposed a novel platform for detecting and monitoring of visual distortion (VD) in macular disorders. In our proposed system, the test data is collected securely from many hospitals as well as individual patients across the world from the comfort of their homes. In this work, we developed the required hardware and software for generating the graphical patterns, displaying the patterns, collecting

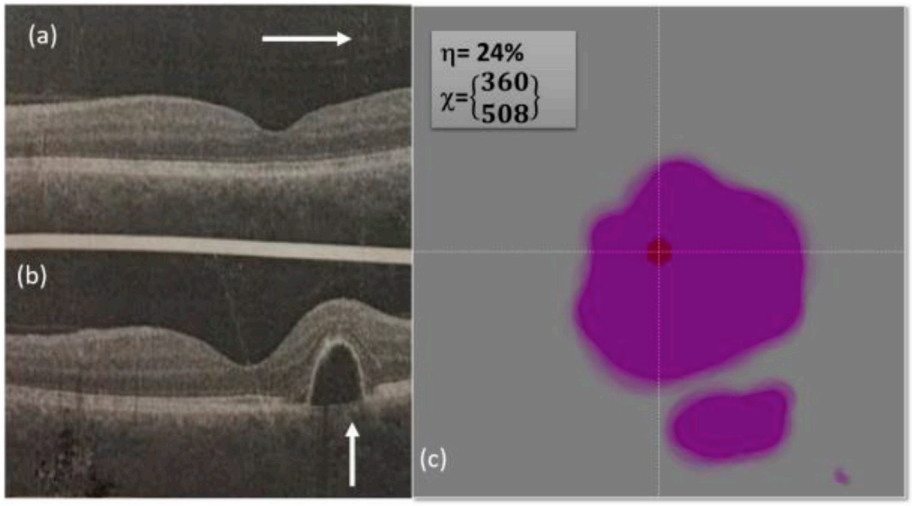

Fig. 20. - Third Macular Disorder Measurement Results of left Eye: (a)–(b) OCT vertical and horizontal OCT images and (c) NGRID heatmap results with η = 24% and χ = (360, 508).

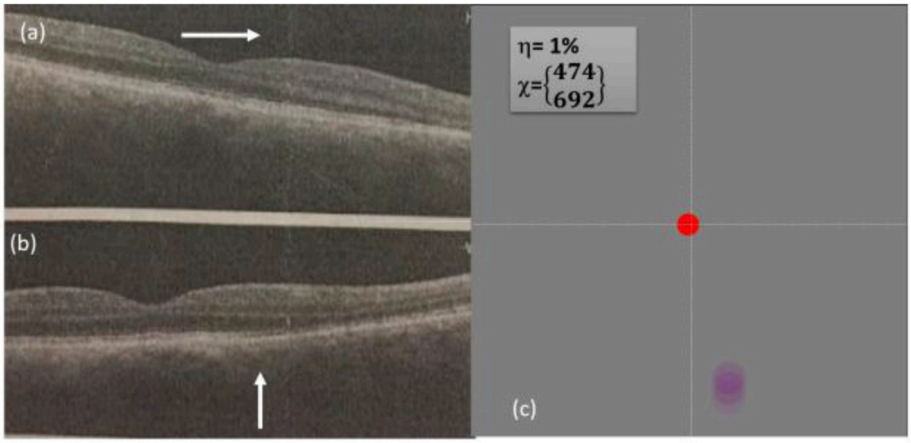

Fig. 21. - Third Macular Disorder Measurement Results of right Eye: (a)–(b) OCT vertical and horizontal OCT images and (c) NGRID heatmap results with η = 1% and χ = (474, 692).

the patients' responses, and creating the associated heatmaps. A visual heatmap of VDs with quantitative measures can provide better indicators compared to traditional VD tests, such as the Amsler chart or other related computerized methods, for eye-care physicians. The NGRID implementation and preliminary measurements and results using healthy participants were also reported to provide an early assessment of systematic errors. The system was also successfully tested and verified on healthy and unhealthy patients. This research is in the process of obtaining the required approval from the Research Ethical Board (REB) in Sunnybrook Hospital, Toronto, Canada, for running a clinical trial on a large number of patients. Therefore, as the continuation of this work, we will test the functionality of the proposed platform for other macular disorders in the future. Furthermore, for achieving the first step in our long-term objective, in the present effort, we have paved the way towards the developments of a novel data platform dedicated to macular disorders by designing and implementing the required software and hardware.

Acknowledgment

Authors would like to thank the support of CMC Microsystem.

References

[1] The Eye Diseases Prevalence Research Group, Prevalence of age-related macular degeneration in the United States, Arch. Ophthalmol. 122 (4) (2004) 564–572.
[2] M. Wang, I.C. Munch, P.W. Hasler, C. Prünte, M. Larsen, Central serous chorioretinopathy, Acta Ophthalmol. 86 (2) (Mar. 2008) 126–145.
[3] J.C. Besharse, D. Bok, The Retina and its Disorders, Academic Press, 2011.
[4] F.G. Holz, R.F. Spaide, Medical Retina: Focus on Retinal Imaging, Springer, 2010.
[5] W.L. Wong, et al., Global prevalence of age-related macular degeneration and disease burden projection for 2020 and 2040: a systematic review and meta-analysis, The Lancet Glob. Health 2 (2) (Feb. 2014) e106–e116.
[6] D.J. Taylor, A.E. Hobby, A.M. Binns, D.P. Crabb, How does age-related macular degeneration affect real-world visual ability and quality of life? A systematic review, BMJ Open 6 (12) (Dec. 2016) e011504.
[7] N.M. Bressler, S.B. Bressler, S.L. Fine, Age-related macular degeneration, Surv. Ophthalmol. 32 (6) (1988) 375–413.
[8] M. Amsler, Earliest symptoms of diseases of the macula, Br. J. Ophthalmol. 37 (9) (1953) 521.
[9] R.A. Schuchard, Validity and interpretation of Amsler grid reports, Arch. Ophthalmol. 111 (6) (Jun. 1993) 776–780.
[10] D.L.C. Isaac, M.P. de Ávila, A.P. Cialdini, Comparison of the original Amsler grid with the preferential hyperacuity perimeter for detecting choroidal neovascularization in age-related macular degeneration, Arq. Bras. Oftalmol. 70 (5) (2007) 771–776.
[11] A. Loewenstein, A. Pollack, A. Schachat, Results of a multicentered, masked clinical trial to evaluate the macular computerized psychophysical test (MCPT) for detection of age-related macular degeneration (AMD), Investig. Ophthalmol. Vis. Sci. 43 (12) (2002) 1213.
[12] M. Crossland, G. Rubin, The Amsler chart: absence of evidence is not evidence of absence, Br. J. Ophthalmol. 91 (3) (Mar. 2007) 391–393.
[13] W. Kohn, J.A. Klingshirn, Characterization and Correction of Macular Distortion, Google Patents, 2014.
[14] A. Loewenstein, et al., Replacing the amsler grid, Ophthalmology 110 (5) (May 2003) 966–970.
[15] V. Lakshminarayanan, J.M. Enoch, Vernier acuity and aging, Int. Ophthalmol. 19 (2) (1995) 109–115.
[16] J.H. Kaas, L.A. Krubitzer, Y.M. Chino, A.L. Langston, E.H. Polley, N. Blair, Reorganization of retinotopic cortical maps in adult mammals after lesions of the retina, Science 248 (4952) (1990) 229–231.
[17] R. Trevino, Recent progress in macular function self-assessment, Ophthalmic Physiol. Optic. 28 (3) (2008) 183–192.
[18] Notal Vision Inc., ForeseeHome, (31-Oct-2015) [Online]. Available: http://www.foreseehome.com , Accessed date: 31 October 2015.
[19] P.M. Fitts, The information capacity of the human motor system in controlling the amplitude of movement, J. Exp. Psychol. 47 (6) (1954) 381.
[20] J.H. Lim, et al., Delay to treatment and visual outcomes in patients treated with anti-vascular endothelial growth factor for age-related macular degeneration, Am. J. Ophthalmol. 153 (4) (Apr. 2012) 678–686 e2.
[21] J. Kim, W. Lee, Stochastic decision making for adaptive crowdsourcing in medical big-data platforms, IEEE Trans. Syst. Man Cybern.: Systems 45 (11) (Nov. 2015) 1471–1476.
[22] Q. Yao, Y. Tian, P.-F. Li, L.-L. Tian, Y.-M. Qian, J.-S. Li, Design and development of a medical big data processing system based on Hadoop, J. Med. Syst. 39 (3) (Feb. 2015) 23.
[23] A. Kaufman, Rendering, Visualization and Rasterization Hardware, Springer Science & Business Media, 1993.
[24] DOM Standard, [Online]. Available: https://dom.spec.whatwg.org/ , Accessed date: 12 September 2018.
[25] E. Samei, et al., Assessment of display performance for medical imaging systems: executive summary of AAPM TG18 report: performance assessment of medical displays, Med. Phys. 32 (4) (Apr. 2005) 1205–1225.
[26] D.H. Kim, Y.J. Lim, D.E. Kim, H. Ren, S.H. Ahn, S.H. Lee, Past, present, and future of fringe-field switching-liquid crystal display, J. Inf. Disp. 15 (2) (Apr. 2014) 99–106.
[27] A.G. Hauptmann, A.I. Rudnicky, A comparison of speech and typed input, Proceedings of the Workshop on Speech and Natural Language - HLT '90, Hidden Valley, Pennsylvania, 1990, pp. 219–224.
[28] Y. Ji, M. Li, X. Zhang, Y. Peng, F. Wen, Poor sleep quality is the risk factor for central serous chorioretinopathy, J Ophthalmol 2018 (2018) 9450297.
[29] T.J. Peiris, H.E. El Rami, J.K. Sun, Central serous chorioretinopathy associated with steroid enema, Retin Cases Brief Rep, Jul. 2018.
[30] A.S. Kitzmann, J.S. Pulido, N.N. Diehl, D.O. Hodge, J.P. Burke, The incidence of central serous chorioretinopathy in Olmsted County, Minnesota, 1980-2002, Ophthalmology 115 (1) (Jan. 2008) 169–173.
[31] C. Arndt, O. Rebollo, S. Séguinet, P. Debruyne, G. Caputo, Quantification of metamorphopsia in patients with epiretinal membranes before and after surgery, Graefe's Arch. Clin. Exp. Ophthalmol. 245 (8) (Jun. 2007) 1123–1129.
[32] N. Yoshimura, Oct-atlas, first ed., Springer, New York, 2013.